REPORT DOCUMENTATION PAGE

Form Approved OMB NO. 0704-0188

1. REPORT DATE (DD-MM-YYYY)	2. REPORT TYPE	3. DATES COVERED (From - To)
30-03-2011	Final Report	1-Mar-2009 - 31-Dec-2010

4. TITLE AND SUBTITLE
Ultra-High Sensitive Magnetoelectric Nanocomposites

5a. CONTRACT NUMBER
W911NF-09-1-0061

5b. GRANT NUMBER

5c. PROGRAM ELEMENT NUMBER
611102

6. AUTHORS
Shashank Priya

5d. PROJECT NUMBER

5e. TASK NUMBER

5f. WORK UNIT NUMBER

7. PERFORMING ORGANIZATION NAMES AND ADDRESSES
Virginia Polytechnic Institute & State University
Office of Sponsored Programs
Virginia Polytechnic Institute and State University
Blacksburg, VA 24060 -

8. PERFORMING ORGANIZATION REPORT NUMBER

9. SPONSORING/MONITORING AGENCY NAME(S) AND ADDRESS(ES)
U.S. Army Research Office
P.O. Box 12211
Research Triangle Park, NC 27709-2211

10. SPONSOR/MONITOR'S ACRONYM(S)
ARO

11. SPONSOR/MONITOR'S REPORT NUMBER(S)
55167-MS.1

12. DISTRIBUTION AVAILIBILITY STATEMENT
Approved for Public Release; Distribution Unlimited

13. SUPPLEMENTARY NOTES
The views, opinions and/or findings contained in this report are those of the author(s) and should not contrued as an official Department of the Army position, policy or decision, unless so designated by other documentation.

14. ABSTRACT
We investigated the synthesis and characterization of magnetoelectric (ME) 3-2 nanocomposite thick films using aerosol-deposition (AD). Piezoelectric and magnetostrictive materials were simultaneously deposited on a platinized silicon substrate using AD method and a 13 micron thick nanocomposite film was realized. Upon annealing, magnetostrictive phase was found to form a layered structure inside the piezoelectric matrix. Detailed microstructural analysis revealed the connectivity of individual phases. This nanocomposite thick film was found to

15. SUBJECT TERMS
magnetoelectric, piezoelectric, laminate, composite, sensor

16. SECURITY CLASSIFICATION OF:			17. LIMITATION OF ABSTRACT	15. NUMBER OF PAGES	19a. NAME OF RESPONSIBLE PERSON
a. REPORT	b. ABSTRACT	c. THIS PAGE			Shashank Priya
UU	UU	UU	UU		19b. TELEPHONE NUMBER: 540-231-0745

Report Title

Ultra-High Sensitive Magnetoelectric Nanocomposites

ABSTRACT

We investigated the synthesis and characterization of magnetoelectric (ME) 3-2 nanocomposite thick films using aerosol-deposition (AD). Piezoelectric and magnetostrictive materials were simultaneously deposited on a platinized silicon substrate using AD method and a 13 micron thick nanocomposite film was realized. Upon annealing, magnetostrictive phase was found to form a layered structure inside the piezoelectric matrix. Detailed microstructural analysis revealed the connectivity of individual phases. This nanocomposite thick film was found to exhibit the ME coefficient of the order of 150 mVcm-1Oe-1 which is significantly higher in comparison to other results reported in literature on ME thin/thick films. For bulk composites, we developed a 2-1-2 magnetoelectric laminate composite having configuration Metglas / PZNT / Metglas with ferrite pillars embedded in the PZNT phase. The piezoelectric layer with composition 0.2Pb(Zn1/3Nb2/3)O3-0.8Pb(Zr0.5Ti0.5)O3 (PZNT) consisted of co-fired (Ni0.6Cu0.2Zn0.2)Fe2O3 (NCZF) pillars. This 2-1-2 composite was found to exhibit the ME coefficient of the order of 352 mV/cm.Oe. Interestingly, the performance of 2-1-2 composite is 15% higher than that of conventional 2-2 laminate composite. Using these composites we developed a broadband ME sensor exhibiting flat response over a wide range of frequency and magnetic DC bias. The sensitivity of bending mode sensor was demonstrated to be 5 nT at room temperature.

List of papers submitted or published that acknowledge ARO support during this reporting period. List the papers, including journal references, in the following categories:

(a) Papers published in peer-reviewed journals (N/A for none)

1. R. A. Islam, V. Bedekar, N. Poudyal, J. P. Liu, and S. Priya, “Magnetoelectric properties of core-shell particulate nanocomposites”, J. Appl. Phys. 104 104111 (2008).
2. V. Bedekar, N. Poudyal, C. B. Rong, J. P. Liu, C. Kim, S. Priya “Improved magnetoelectric properties of piezoelectric-magnetostrictive nanocomposites synthesized using high-pressure compaction technique”, J. Mater. Sci. 44, 2162-2166 (2009).
3. R. Islam, Y. Ni, A. Khachaturyan, and S. Priya, “Giant magnetoelectric effect in sintered multilayered composite structures”, J. Appl. Phys. 104, 044103 (2008).
4. R. A. Islam, C.-b. Rong, J. P. Liu and S. Priya, “Gradient Composite Structure in Cofired Bilayer Magnetoelectric Composites of Pb(Zr0.56Ti0.44)O3 - Ni0.6Zn0.2Cu0.2Fe2O4 System” J. Mater. Sci. Lett. 43, 6337-6343 (2008).
5. R. Islam and S. Priya, “ME Response of Cofired Trilayer Magnetoelectric Composites with Partial Texturing”, J. Mater. Sci., (2009) DOI 10.1007/s10853-009-3744-9.
6. R. A. Islam, and S. Priya, “Effect of piezoelectric grain size on magnetoelectric coefficient of Pb(Zr0.52Ti0.48)O3-Ni0.8Zn0.2Fe2O4 particulate composites”, J. Mater. Sci. 43, 3560 – 3568 (2008).
7. R. Islam, and S. Priya, “Large magnetoelectric coefficient in Co-fired Pb (Zr0.52Ti0.48)O3–Pb (Zn1/3Nb2/3)O3–Ni0.6Cu0.2Zn0.2Fe2O4 trilayer magnetoelectric composites”, J. Mater. Sci. 43, 2072 – 2076 (2008).
8. R. A. Islam, D. Viehland, and S. Priya, “Doping effect on magnetoelectric coefficient of Pb(Zr052Ti0.48)O3-Ni(1-x)ZnxFe2O4 particulate composite”, J. Mater. Sci. 43, 1497 – 1500 (2008).
9. R. Islam and S. Priya, “ME Response of Cofired Trilayer Magnetoelectric Composites with Partial Texturing”, J. Mater. Sci., (2009) (accepted).
10. C.-S. Park, C.-W. Ahn, J. Ryu, W.-H. Yoon, D.-S. Park, H.-E. Kim, and S. Priya, “Design and Characterization of Broadband Magnetoelectric Sensor” J. Appl. Phys., 105, 094111 (2009).
11. C.-S. Park, J. Ryu, J.-J. Choi, D.-S. Park, and S. Priya, “Giant Magnetoelectric Coeffeicient in 3-2 Nanocomposite Thick Films” Jpn. J. Appl. Phys., 48, 080204 (2009).
12. J. Ryu, C.-S. Park, J.-J. Choi, B.-D. Hahn, W.-Ha Yoon, B.-Kuk Lee, D.-Soo Park, S. Priya, K.-Young Kim, and C. Park, “Dielectric Behavior of Aerosol Deposited Mn-modified PZT-PZN Thick Films”, Philosophical Mag. Lett. 89, 665 (2009).
13. J. Ryu, S. Priya, C.-Sung Park, K.-Young Kim, J.-Jin Choi, B.-Dong Hahn, W.-Ha Yoon, B.-Kuk Lee, D.-Soo Park, and C. Park, “Enhanced Domain Contribution to Ferroelectric Properties in Free-Standing Thick Films”, J. Appl. Phys. 106, 024108 (2009).
14. C.-S. Park, C.-W. Ahn, S. C. Yang and S. Priya, “Dimensionally Gradient Magnetoelectric Bimorph Structure Exhibiting Wide Frequency and Magnetic DC Bias Operating Range”, J. Appl. Phys. 106, 114101 (2009).
15. V. Bedekar, R. A. Islam, H. Kim, M. I. Bichurin, S. N. Ivanov, Y. J. Pukinski and S. Priya, “Magnetoelectric Gradiometer”, EURO. PHYS. J. B 71, 387-392 (2009).
16. V. Bedekar, G. Singh, Roop L Mahajan, and S. Priya, Synthesis and Microstructural Characterization of Barium Titanate Nanoparticles Decorated SiCN-MWCNT Nanotubes – “nanoNecklace”, Ferroelect. Lett. Sect. 36, 133-140 (2009).
17. S. Priya, J. Ryu, C.-S. Park, J. Oliver, J.-J. Choi and D.-S. Park, “Piezoelectric and Magnetoelectric Thick Films for Fabricating Power Sources in Wireless Sensor Nodes,” Sensors, 9 (8), 6362-6384 (2009).
18. C.-S. Park, C.-W. Ahn, and S. Priya, “Enhanced Magnetoelectric Properties in Three Phase Composites with 2-1-2 connectivity,” Philosophical Magazine, 90, [No.33, 21] (2010).
19. C.-S. Park, D. Avirovik, S. Bressers, and S. Priya, “Low-Frequency NanoTesla Sensitivity in Metglas / Piezoelectric / Carbon Fiber / Piezoelectric Composites with Active Tip-Mass,” Appl. Phys. Lett., 98 062904 (2011).

Number of Papers published in peer-reviewed journals: 19.00

(b) Papers published in non-peer-reviewed journals or in conference proceedings (N/A for none)

Number of Papers published in non peer-reviewed journals: 0.00

(c) Presentations

S. Priya, C.-S. Park, V. Bedekar, J. Ryu, D.-S. Park "Magnetoelectric Particulate Composites," MS&T '09 in Pittsburgh, Pennsylvania, USA, Oct. 25-29th, (2009).
2. C.-S. Park, C.-W. Ahn, and S. Priya, "Synthesis of magnetoelectric composites with varying connectivity using tape casting approach," MS&T '09 in Pittsburgh, Pennsylvania, USA, Oct. 25-29th, (2009).
3. C.-S. Park, C.-W. Ahn, and S. Priya, "Co-fired Magnetoelectric Laminate Composite," EMA2010, Jan. 20-22, FL, USA (2010).
4. C.-S. Park, C.-W. Ahn, S.-C. Yang, and S. Priya, "Broad/Wide Band Magnetoelectric Sensor: Current State and Challenge," EMA2010, Jan. 20-22, FL, USA (2010).
5. C.-S. Park, S.-C. Yang, C.-W. Ahn, and S. Priya, "Enhanced Magnetoelectric Properties in Three Phase Composites with 2-1-2 Connectivity," IWPMA2010, Oct. 10-13, Antalya, Turkey (2010).
6. C.-S. Park and S. Priya, "Design and Characterization of Magnetoelectric Composites," NSF INAMM (International Symposium on Multifunctionality of Ferroics and Multiferroics), Oct. 15-16, UTSA, San Antonio, TX, USA (2010).
7. (Invited) C.-S. Park, S.-C. Yang, K.-H. Cho, and S. Priya, "Magnetoelectric Response of Composites with Varying Connectivity," MS&T2010, Oct. 17-21, George R. Brown Convention Center, Houston, TX, USA (2010).
8. C.-S. Park, K.-H. Cho, S.-C. Yang, and S. Priya, "Enhanced Magnetoelectric Properties at Low Frequency Bending Mode Resonance," Electronic Materials and Applications 2011, Jan. 19-21, Orlando, FL, USA (2011).
9. V. Bedekar, M. I. Bichurin, S. N. Ivanov, Y. J. Pukinski, H. Kim,
R. A. Islam, and S. Priya, "Magnetoelectric Gradiometer", MEIPIC6 workshop 2009.
10. C. Park, H. Kim, R. Mahajan, S. Priya, "Multilayer Magnetoelectric Nanostructures of CoFe2O4 – BaTiO3", MS&T'08 (October 5 – 9, 2008, David L. Lawrence Convention Center, Pittsburg, PA).
11. R. Islam, N. Podual, J. P. Liu, C. Kim, S. Priya, "Synthesis of Layered Magnetoelectric Composites through "Bottom-Up" Approach", MS&T'08 (October 5 – 9, 2008, David L. Lawrence Convention Center, Pittsburg, PA).
12. Invited talk, S. Priya, Magnetoelectric Composites, 2009 MRS Spring Meeting, San Francisco, CA, April 13 – 17 (Symposia I: Multiferroics and Magnetoelectrics).
13. Invited presentation, S. Priya, "Structure - property relationships in perovskite - spinel based magnetoelectric composites", The Rank Prize Funds Mini-Symposium on Periodically-Modulated and Artificially Hetero-Structured Devices Wordsworth Hotel, Grasmere, Cumbria LA22 9SW, UK, 18th to 21st May 2009.
13. R. A. Islam, and S. Priya, "Grain Size dependence of magnetoelectric coefficient in Pb(Zr0.52Ti0.48)O3 – 0.2Ni0.8Zn0.2Fe2O4 System", 109th Annual Meeting of The American Ceramic Society combined with MS&T'07, September 16 – 20, Detroit, MI, (2007).
14. R. B. Mahajan, H. Kim, R. Islam, M. Karmakar, and S. Priya, "Multilayer magnetoelectric nanostructures of CoFe2O4 – BaTiO3", 109th Annual Meeting of The American Ceramic Society combined with MS&T'07, September 16 – 20, Detroit, MI, (2007).

Number of Presentations: 14.00

Non Peer-Reviewed Conference Proceeding publications (other than abstracts):

Number of Non Peer-Reviewed Conference Proceeding publications (other than abstracts): 0

Peer-Reviewed Conference Proceeding publications (other than abstracts):

Number of Peer-Reviewed Conference Proceeding publications (other than abstracts): 0

(d) Manuscripts

1.C.-S. Park and S. Priya, "Co-fired Magnetoelectric Laminate Composite," J. Am. Ceram. Soc., Online Published DOI: 10.1111/j.1551-2916.2010.04213.x.

2. C.-S. Park, J. Evans, and S. Priya, "Quantitative Understanding of Elastic Coupling in Magnetoelectric ," Smart Mater. Struct. (2011).

Number of Manuscripts: 2.00

Patents Submitted

Patents Awarded

Awards

1. Deans award for excellence in research, college of engineering, Virginia Tech

Graduate Students

NAME	PERCENT_SUPPORTED
Su Chul Yang	
FTE Equivalent:	
Total Number:	**1**

Names of Post Doctorates

NAME	PERCENT_SUPPORTED
Chee-Sung Park	0.50
FTE Equivalent:	**0.50**
Total Number:	**1**

Names of Faculty Supported

NAME	PERCENT_SUPPORTED	National Academy Member
Shashank Priya	0.00	No
Choongun Kim	0.10	No
FTE Equivalent:	**0.10**	
Total Number:	**2**	

Names of Under Graduate students supported

NAME	PERCENT_SUPPORTED
FTE Equivalent:	
Total Number:	

Student Metrics

This section only applies to graduating undergraduates supported by this agreement in this reporting period

The number of undergraduates funded by this agreement who graduated during this period:	0.00
The number of undergraduates funded by this agreement who graduated during this period with a degree in science, mathematics, engineering, or technology fields:.....	0.00
The number of undergraduates funded by your agreement who graduated during this period and will continue to pursue a graduate or Ph.D. degree in science, mathematics, engineering, or technology fields:.....	0.00
Number of graduating undergraduates who achieved a 3.5 GPA to 4.0 (4.0 max scale):	0.00
Number of graduating undergraduates funded by a DoD funded Center of Excellence grant for Education, Research and Engineering:	0.00
The number of undergraduates funded by your agreement who graduated during this period and intend to work for the Department of Defense	0.00
The number of undergraduates funded by your agreement who graduated during this period and will receive scholarships or fellowships for further studies in science, mathematics, engineering or technology fields:	0.00

Names of Personnel receiving masters degrees

NAME

Total Number:

Names of personnel receiving PHDs

NAME
Rashed Islam
Vishwas Bedekar
Total Number: 2

Names of other research staff

NAME	PERCENT_SUPPORTED
FTE Equivalent:	
Total Number:	

Sub Contractors (DD882)

1 a. University of Texas at Arlington

1 b. Research Administration
The University of Texas at Arlington
Arlington TX 760190145

Sub Contractor Numbers (c):
Patent Clause Number (d-1):
Patent Date (d-2):
Work Description (e):
Sub Contract Award Date (f-1):
Sub Contract Est Completion Date(f-2):

---

1 a. University of Texas at Arlington

1 b. P. O. Box 19145
Office of Sponsored Projects
Arlington TX 76019

Sub Contractor Numbers (c):
Patent Clause Number (d-1):
Patent Date (d-2):
Work Description (e):
Sub Contract Award Date (f-1):
Sub Contract Est Completion Date(f-2):

Inventions (DD882)

Scientific Progress

See Attachment

Technology Transfer

Title: Ultra-High Sensitive Magnetoelectric Nanocomposite Current Sensors

Funding number: W911NF0910061

Agency report number: 55167MS

Authors: Shashank Priya

Reporting period: August 2009 – Jan. 2011

(1)List of papers submitted or published under ARO sponsorship.

Manuscript published in peer-reviewed journals

1. R. A. Islam, V. Bedekar, N. Poudyal, J. P. Liu, and S. Priya, "Magnetoelectric properties of core-shell particulate nanocomposites", J. Appl. Phys. 104 104111 (2008).
2. V. Bedekar, N. Poudyal, C. B. Rong, J. P. Liu, C. Kim, S. Priya "Improved magnetoelectric properties of piezoelectric-magnetostrictive nanocomposites synthesized using high-pressure compaction technique", J. Mater. Sci. 44, 2162-2166 (2009).
3. R. Islam, Y. Ni, A. Khachaturyan, and S. Priya, "Giant magnetoelectric effect in sintered multilayered composite structures", J. Appl. Phys. 104, 044103 (2008).
4. R. A. Islam, C.-b. Rong, J. P. Liu and S. Priya, "Gradient Composite Structure in Cofired Bilayer Magnetoelectric Composites of $Pb(Zr_{0.56}Ti_{0.44})O_3$ - $Ni_{0.6}Zn_{0.2}Cu_{0.2}Fe_2O_4$ System" J. Mater. Sci. Lett. 43, 6337-6343 (2008).
5. R. Islam and S. Priya, "ME Response of Cofired Trilayer Magnetoelectric Composites with Partial Texturing", J. Mater. Sci., (2009) DOI 10.1007/s10853-009-3744-9.
6. R. A. Islam, and S. Priya, "Effect of piezoelectric grain size on magnetoelectric coefficient of $Pb(Zr_{0.52}Ti_{0.48})O_3$-$Ni_{0.8}Zn_{0.2}Fe_2O_4$ particulate composites", J. Mater. Sci. 43, 3560 – 3568 (2008).
7. R. Islam, and S. Priya, "Large magnetoelectric coefficient in Co-fired Pb $(Zr_{0.52}Ti_{0.48})O_3$–Pb $(Zn_{1/3}Nb_{2/3})O_3$–$Ni_{0.6}Cu_{0.2}Zn_{0.2}Fe_2O_4$ trilayer magnetoelectric composites", J. Mater. Sci. 43, 2072 – 2076 (2008).
8. R. A. Islam, D. Viehland, and S. Priya, "Doping effect on magnetoelectric coefficient of $Pb(Zr_{052}Ti_{0.48})O_3$-$Ni_{(1-x)}Zn_xFe_2O_4$ particulate composite", J. Mater. Sci. 43, 1497 – 1500 (2008).
9. R. Islam and S. Priya, "ME Response of Cofired Trilayer Magnetoelectric Composites with Partial Texturing", J. Mater. Sci., (2009) (accepted).
10. C.-S. Park, C.-W. Ahn, J. Ryu, W.-H. Yoon, D.-S. Park, H.-E. Kim, and S. Priya, "Design and Characterization of Broadband Magnetoelectric Sensor" *J. Appl. Phys*., **105**, 094111 (2009).
11. C.-S. Park, J. Ryu, J.-J. Choi, D.-S. Park, and S. Priya, "Giant Magnetoelectric Coeffeicient in 3-2 Nanocomposite Thick Films" *Jpn. J. Appl. Phys.,* 48, 080204 (2009).
12. J. Ryu, C.-S. Park, J.-J. Choi, B.-D. Hahn, W.-Ha Yoon, B.-Kuk Lee, D.-Soo Park, S. Priya, K.-Young Kim, and C. Park, "Dielectric Behavior of Aerosol

Deposited Mn-modified PZT-PZN Thick Films", Philosophical Mag. Lett. 89, 665 (2009).

13. J. Ryu, S. Priya, C.-Sung Park, K.-Young Kim, J.-Jin Choi, B.-Dong Hahn, W.-Ha Yoon, B.-Kuk Lee, D.-Soo Park, and C. Park, "Enhanced Domain Contribution to Ferroelectric Properties in Free-Standing Thick Films", J. Appl. Phys. 106, 024108 (2009).
14. C.-S. Park, C.-W. Ahn, S. C. Yang and S. Priya, "Dimensionally Gradient Magnetoelectric Bimorph Structure Exhibiting Wide Frequency and Magnetic DC Bias Operating Range", J. Appl. Phys. 106, 114101 (2009).
15. V. Bedekar, R. A. Islam, H. Kim, M. I. Bichurin, S. N. Ivanov, Y. J. Pukinski and S. Priya, "Magnetoelectric Gradiometer", EURO. PHYS. J. B 71, 387-392 (2009).
16. V. Bedekar, G. Singh, Roop L Mahajan, and S. Priya, Synthesis and Microstructural Characterization of Barium Titanate Nanoparticles Decorated SiCN-MWCNT Nanotubes – "nanoNecklace", Ferroelect. Lett. Sect. 36, 133-140 (2009).
17. S. Priya, J. Ryu, C.-S. Park, J. Oliver, J.-J. Choi and D.-S. Park, "Piezoelectric and Magnetoelectric Thick Films for Fabricating Power Sources in Wireless Sensor Nodes," *Sensors*, ***9*** (8), 6362-6384 (2009).
18. C.-S. Park, C.-W. Ahn, and S. Priya, "Enhanced Magnetoelectric Properties in Three Phase Composites with 2-1-2 connectivity," *Philosophical Magazine,* **90**, [No.33, 21] (2010).
19. C.-S. Park, D. Avirovik, S. Bressers, and S. Priya, "Low-Frequency NanoTesla Sensitivity in Metglas / Piezoelectric / Carbon Fiber / Piezoelectric Composites with Active Tip-Mass," *Appl. Phys. Lett.,* **98** 062904 (2011).

Manuscript accepted for publication

1. C.-S. Park and S. Priya, "Co-fired Magnetoelectric Laminate Composite," J. Am. Ceram. Soc., **Online Published** DOI: 10.1111/j.1551-2916.2010.04213.x.

Manuscript submitted not published

1. C.-S. Park, J. Evans, and S. Priya, "Quantitative Understanding of Elastic Coupling in Magnetoelectric ," *Smart Mater. Struct.* (2011).

Papers presented at meetings, but not published in conference proceedings

1. S. Priya, C.-S. Park, V. Bedekar, J. Ryu, D.-S. Park "Magnetoelectric Particulate Composites," MS&T '09 in Pittsburgh, Pennsylvania, USA, Oct. 25-29th, (2009).
2. C.-S. Park, C.-W. Ahn, and S. Priya, "Synthesis of magnetoelectric composites with varying connectivity using tape casting approach," MS&T '09 in Pittsburgh, Pennsylvania, USA, Oct. 25-29th, (2009).
3. C.-S. Park, C.-W. Ahn, and S. Priya, "Co-fired Magnetoelectric Laminate Composite," EMA2010, Jan. 20-22, FL, USA (2010).
4. C.-S. Park, C.-W. Ahn, S.-C. Yang, and S. Priya, "Broad/Wide Band Magnetoelectric Sensor: Current State and Challenge," EMA2010, Jan. 20-22, FL, USA (2010).

5. C.-S. Park, S.-C. Yang, C.-W. Ahn, and S. Priya, "Enhanced Magnetoelectric Properties in Three Phase Composites with 2-1-2 Connectivity," IWPMA2010, Oct. 10-13, Antalya, Turkey (2010).
6. C.-S. Park and S. Priya, "Design and Characterization of Magnetoelectric Composites," NSF INAMM (International Symposium on Multifunctionality of Ferroics and Multiferroics), Oct. 15-16, UTSA, San Antonio, TX, USA (2010).
7. **(Invited)** C.-S. Park, S.-C. Yang, K.-H. Cho, and S. Priya, "Magnetoelectric Response of Composites with Varying Connectivity," MS&T2010, Oct. 17-21, George R. Brown Convention Center, Houston, TX, USA (2010).
8. C.-S. Park, K.-H. Cho, S.-C. Yang, and S. Priya, "Enhanced Magnetoelectric Properties at Low Frequency Bending Mode Resonance," Electronic Materials and Applications 2011, Jan. 19-21, Orlando, FL, USA (2011).
9. V. Bedekar, M. I. Bichurin, S. N. Ivanov, Y. J. Pukinski, H. Kim, R. A. Islam, and S. Priya, "Magnetoelectric Gradiometer", MEIPIC6 workshop 2009.
10. C. Park, H. Kim, R. Mahajan, S. Priya, "Multilayer Magnetoelectric Nanostructures of $CoFe_2O_4$ – $BaTiO_3$", *MS&T'08 (October 5 – 9, 2008, David L. Lawrence Convention Center, Pittsburg, PA).*
11. R. Islam, N. Podual, J. P. Liu, C. Kim, S. Priya, "Synthesis of Layered Magnetoelectric Composites through "Bottom-Up" Approach", *MS&T'08 (October 5 – 9, 2008, David L. Lawrence Convention Center, Pittsburg, PA).*
12. Invited talk, S. Priya, Magnetoelectric Composites, 2009 MRS Spring Meeting, San Francisco, CA, April 13 – 17 (Symposia I: Multiferroics and Magnetoelectrics).
13. Invited presentation, S. Priya, "Structure - property relationships in perovskite - spinel based magnetoelectric composites", The Rank Prize Funds Mini-Symposium on Periodically-Modulated and Artificially Hetero-Structured Devices Wordsworth Hotel, Grasmere, Cumbria LA22 9SW, UK, 18th to 21st May 2009.
13. R. A. Islam, and S. Priya, "Grain Size dependence of magnetoelectric coefficient in $Pb(Zr_{0.52}Ti_{0.48})O_3$ – $0.2Ni_{0.8}Zn_{0.2}Fe_2O_4$ System", 109th Annual Meeting of The American Ceramic Society combined with MS&T'07, September 16 – 20, Detroit, MI, (2007).
14. R. B. Mahajan, H. Kim, R. Islam, M. Karmakar, and S. Priya, "Multilayer magnetoelectric nanostructures of $CoFe_2O_4$ – $BaTiO_3$", 109th Annual Meeting of The American Ceramic Society combined with MS&T'07, September 16 – 20, Detroit, MI, (2007).

(1) Demographic data for this reporting period

1. Number of manuscript submitted during this program – 21
2. Number of peer-reviewed papers submitted during this reporting period – 21
3. Number of Non-peer reviewed papers submitted during this reporting period – 0
4. Number of presented but not published papers submitted during this reporting period – 14

(2) Demographic Data for the life of this agreement:

1. Number of PhD(s) awarded as a result of this agreement – 2
2. Number of Grad Students supported by this agreement – 4.5
3. Number of post doctorates supported by this agreement – 1
4. Number of faculty supported by this agreement – 3

Scientific progress and accomplishments (since last report)

I. Synthesis of PZT-PZN & PZT-PZN-Mn Thick Film

A 10µm-thick piezoelectric films were synthesized using aerosol deposition (AD) process. The AD method is a promising way to fabricate thick films with dense microstructure. Furthermore, the effect of Mn-doping in synthesized thick films under low and high field drives was investigated. The base composition of films was selected as $0.9Pb(Zr_{0.52}Ti_{0.48})O_3$-$0.1Pb(Zn_{1/3}Nb_{2/3})O_3$ (PZT-PZN), which was modified with Mn as $0.9Pb(Zr_{0.52}Ti_{0.48})O_3$-$0.1Pb(Zn_{1/3}Nb_{2/3})O_3$-0.52 wt% MnO_2 (PZT-PZN-Mn) to induce a hardening effect. Figure I.1 shows the X-ray diffraction (XRD) patterns of initial starting powders and annealed films. The initial starting powders as well as deposited films showed perovskite structure with no trace of any secondary phase.

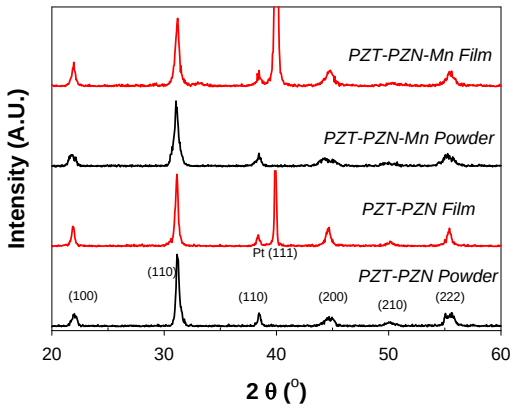

Figure I.1. XRD Patterns of the powders and thick films of PZT-PZN and PZT-PZN-Mn.

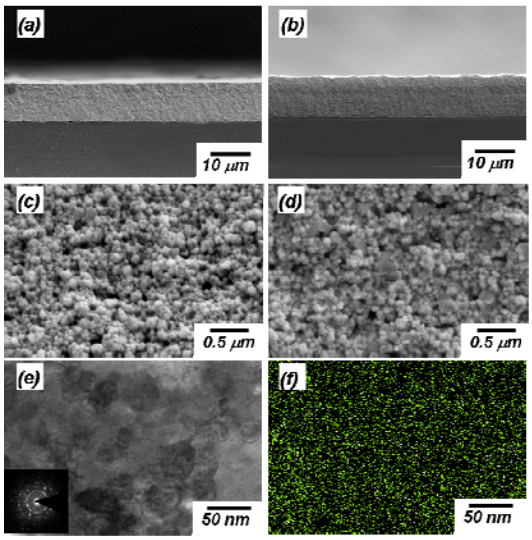

Figure I.2. SEM cross sectional micrographs of (a) PZT-PZN, (b) PZT-PZN-Mn, higher magnification cross sectional micrographs of fractured (c) PZT-PZN, and (d) PZT-PZN-Mn, (e) TEM micrograph and SAED pattern of PZT-PZN-Mn, and (f) the distribution of Mn by EDX mapping based on (f).

Figures I.2 (a) and (b) show the cross-section of PZT-PZN and PZT-PZN-Mn films

illustrating dense microstructure and good adhesion with substrate. The thickness of films was estimated to be in the vicinity of 10 µm. Figures I.2 (c) and (d) show the high magnification fractured cross-sectional microstructures of the PZT-PZN and PZT-PZN-Mn film where grain size was found to be in the wide range of 10 – 100 nm. The microstructure of both Mn-doped and undoped PZT-PZN were found to be identical in terms of grain size and heterogeneity. Transmission electron microscopy (TEM) image and selected area electron diffraction (SAED) pattern of PZT-PZN-Mn film shown in Fig. I.2(e) revealed the distribution of crystallites with a size range of several tens of nanometer and no trace of amorphous phase. In addition, two dimensional energy dispersive spectrometer (EDS) mapping of Mn element was conducted on Fig. I.2 (e), and it showed a uniform distribution of Mn element as shown in Fig. I.2 (f). These results indicate that PZT-PZN and PZT-PZN-Mn films were of the same thickness, crystallinity, and density. Thus, the changes in dielectric and ferroelectric behaviors could be attributed to Mn-doping directly.

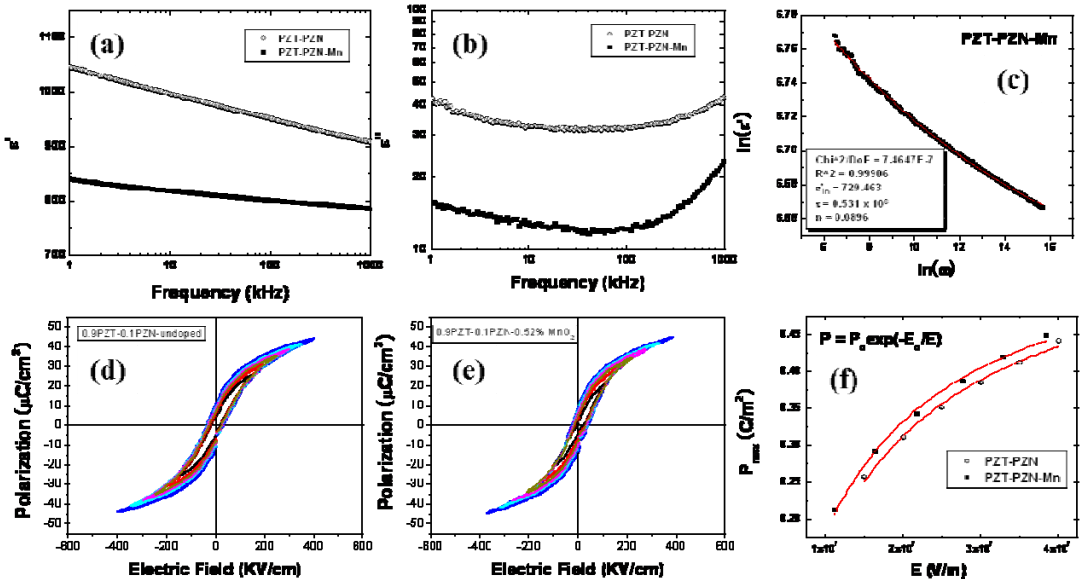

Figure I.3. (a) Dielectric constant and (b) dielectric loss factor of PZT-PZN and PZT-PZN-Mn films as a function of frequency, (c) Fitting of dielectric data using power law, Polarization as a function of electric field for (d) PZT-PZN and (e) PZT-PZN-Mn films. (f) Fitting of maximum polarization using modified Arrhenius equation.

Dielectric constant (ε') and loss factor (tanδ = ε"/ε') of the PZT-PZN and PZT-PZN-Mn films were measured as a function of frequency. Figures I.3(a) and (b) show the variation of real and imaginary parts of the dielectric constant as a function of frequency, respectively. There is clearly significant reduction in both real and imaginary parts for PZT-PZN-Mn films indicating the reduced extrinsic contribution. Defects and substituents are known to affect the dielectric properties of the ferroelectrics in both poled and unpoled conditions. In general there are two types of defects, mobile defects and randomly quenched defects. Mobile defects are known to induce hard piezoelectric behavior whereas randomly quenched ones induce soft behavior. The hard properties resulted from the distribution of Mn^{2+} onto the B-sites. Mn^{2+} incorporated onto the B sites

would act as a lower valent species on a higher valent site. Accordingly, oxygen vacancies would be created for charge compensation, imparting polarization pinning and "hard" characteristics. This may effectively pin the 180° domain motion resulting in reduced dielectric loss and dielectric constant. It is well known that the 180° domain has smaller internal stress than the 90° domain in the switching process. Oxygen vacancies or point defects can easily migrate to the domain boundaries, form clusters, and result in a pinned polarization state. Therefore, 180° domain motion is more easily influenced and inhibited by those defects. This can be easily explained from the results of Figs. I.3(a) and (b).

The polarization dynamics in PZT-PZN-Mn thin films can be modeled analogous to magnetic glassy systems. Previously, we have shown for the PMN-PT system that piezoelectric relaxation is a stretched exponential that is superimposed upon a purely logarithmic decay term derived using the droplet model for spin glass systems below their freezing temperature. The form of this relationship is given in the equation in terms of d_{33} as:

$$d_{33} = A_1 \exp[-(t/\tau_o)^n] + (d_{33}(o) - A_2 \ln(t) \qquad \text{(I.1)}$$

where τ_o is a characteristic relaxation time, A_1 is the non-equilibrium relaxation rate, A_2 is the relaxation rate in dynamical equilibrium, and n is an exponent. Conventionally, for the single relaxation time i.e. there are no appreciable dynamic correlations on a longer time scale; the relaxation rate is given by Debye relation:

$$R(t) \sim \exp(-t\omega) \qquad \text{(I.2)}$$

In the disordered systems, the distributed relaxation time will be the average of the clusters and expressed using the power law as:

$$\varepsilon' = \varepsilon'_{in} \exp\left[\left(\frac{1}{\omega\tau}\right)^n\right] \qquad \text{(I.3)}$$

where ε'_{in} is the frequency independent dielectric constant, τ is the relaxation time and n is the dimensionality. Equation (I.3) can be expressed in terms of logarithmic variables as:

$$\ln \varepsilon' = \ln \varepsilon'_{in} + A_1 \exp\left[-\frac{\ln \omega}{t_1}\right] \qquad \text{(I.4)}$$

where $t_1 = 1/n$, and $A_1 = (1/\tau)^n$. Figure I.3(c) shows the logarithmic variation of the real part of dielectric constant with frequency for PZT-PZN-Mn films. The data in this figure was fitted by Eq. (I.4) and the fitted curve is shown by a solid line. The fitted parameters were found to be as: $\varepsilon'_{in} = 729$, $\tau = 0.53 \times 10^6$s, and $n = 0.089$. Similar analysis on the PZT-PZN films yielded the coefficients as: $\varepsilon'_{in} = 885$, $\tau = 5.72$s, and $n = 0.178$. Comparing the magnitudes of the frequency independent term and relaxation times, it can be seen that Mn doping significantly reduces the dynamics of the system, that means the hardening effect by Mn doping was clearly observed. It is known that in a disordered system, defects have a tendency to cluster at the domain boundaries and provide the pinning sites for polarization. Polarization reversal in such systems has been found to occur by the heterogeneous nucleation and growth process in the vicinity of quenched

random defects. Accordingly, switching occurs by the creation of fractal domains (i.e., nuclei or small clusters of reversed polarization within a poled condition). In such systems, even a small concentration of impurity makes a large contribution to the random fields (if the domain polarization is parallel to the local fluctuations of the random fields) and may have strong influence on the pinning of the domain boundaries and a much higher field is required to destabilize the domain boundaries. To further elucidate this point, we next investigated the polarization behavior under high field – low frequency conditions.

Figures I.3(d) and (e) show the field dependent P–E loops for PZT-PZN and PZT-PZN-Mn, respectively. Comparing the P-E loops for pure and modified PZT-PZN in fully saturated condition, it can be seen that there is asymmetric shift indicative of internal bias field. The magnitude of coercive fields E_c^- and E_c^+ for PZT-PZN were found to be -37.2 and 30.0 kV/cm, while for PZT-PZN-Mn they were found to be -24.8 and 41.2 kV/cm. Using these values the bias field can be calculated to be -3.6 kV/cm for PZT-PZN and 8.18 for PZT-PZN-Mn. For the PZT-PZN film, the internal bias might be derived from the stress between the film and substrate. It is well known that the stress is one of the origins for imprint phenomena. On the other hand for Mn-doped PZT-PZN, the imprint was from the internal bias generated by the acceptor. This confirms the presence of domain wall pinning effects by defect dipoles which oppose the change in polarization. The variation of the saturated polarization (P_{max}) with amplitude of applied electric field is shown in Fig. I.3(f). The polarization variation was modeled using the modified Arrhenius equation, given as:

$$P = P_o \exp\left(-\frac{E_o}{E}\right) \qquad \text{(I.5)}$$

where P_o is the polarization magnitude of the nuclei and E_o is the activation field required to depin the domain boundaries. This is consistent with the fact that the macroscopic relaxation phenomenon is the summed average of the microscopic relaxation processes. The magnitude of P_o and E_o for PZT-PZN-Mn film was found to be 0.601 C/m^2 and 1.187×10^7 V/m respectively. Fitting Eq.(I.5) to the pure PZT-PZN film yielded the magnitude of P_o and E_o as 0.601 and 1.311×10^7 V/m respectively. These magnitudes are quite similar indicating that at higher fields defect clusters collapse and no longer act as the pinning source. These high quality thick ferroelectric films provide baseline for development of the high performance magnetoelectric films.

II. New magnetoelectric nano-structure design (3-2 connectivity)

A new-typed ME nanocomposite thick films was successfully synthesized using aerosol deposition (AD). We pursued the synthesis of ME 3-2 nanocomposite thick films which is a partially laminated structure in the matrix comprising of ferroelectric and magnetostrictive phases using AD. The schematic diagram of the AD process is shown in Fig. II.1 (a). After annealing at 700°C for 1 h, the resulting structure shown schematically in Fig. II.1 (b) was obtained. NCZF phases with 2D connectivity were dispersed in the PZNT matrix. It can be noted in this figure that connectivity of ferrite is complex, which is difficult to be achieved by other processes.

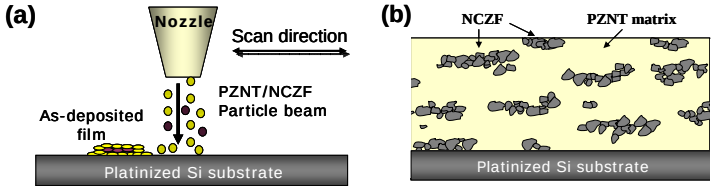

Fig. II.1. (a) Schematic description of aerosol deposition process used for synthesizing nanocomposite films, (b) Schematic microstructure of the resulting film

Figure II.2(a) shows the XRD patterns of initial starting powders, as-deposited film, and annealed film. The powders showed co-existence of perovskite (PZNT) and spinel (NCZF) phases with sharp peaks, while the as-deposited films exhibited broad peaks due to its nanocrystalline structure. Upon annealing the films at 700°C, a polycrystalline composite with mixture of perovskite and spinel phases was obtained.

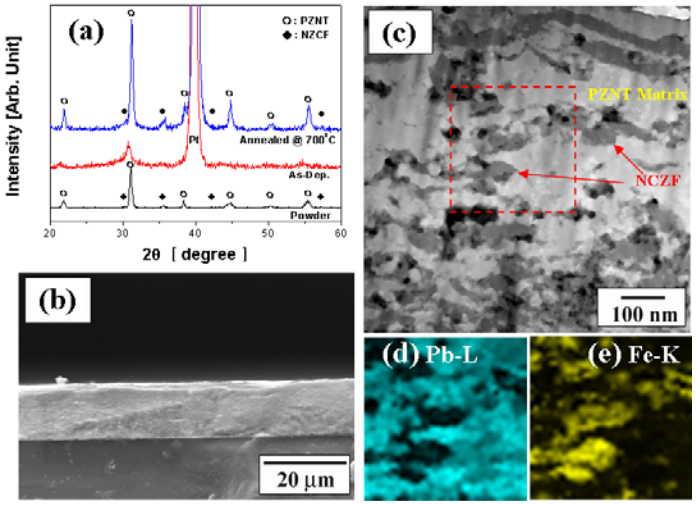

Fig. II.2. (a) XRD patterns of the powders and composite thick films, (b) cross-sectional SEM image, (c) STEM, (d) and (e) EDX mapping.

Figure II.2(b) shows the cross-section of ME composite films illustrating dense microstructure and good adhesion with the substrate. The thickness of films was estimated to be in the vicinity of 13μm. STEM microstructure is shown in Fig. II.2(c). NCZF phases were partially laminated in the PZNT matrix. The results of EDX mapping for the marked area in Fig. II.2(c) is shown in Fig. II.2 (d) and (e) for elements Pb and Fe representing the PZNT and NCZF phases, respectively.

ME properties of 3-2 nanocomposites were measured in longitudinal - transverse (L-T) mode. The maximum ME output voltage was found to be 150 mV/cm.Oe, as shown in Fig. II.3. This high ME response was resulted in a reduced clamping effect in 13μm thick films, effective poling of the piezoelectric matrix, and enhanced elastic coupling.

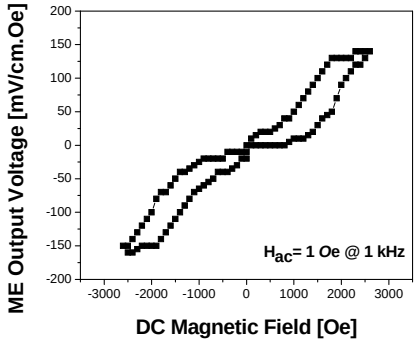

Fig. II.3. ME coefficient of 3-2 ME composite film with PZNT-NCZF fabricated by AD as a function of DC magnetic bias field.

III. Broadband Magnetoelectric ME sensor (Design & Characterization)

We have recently reported a design for broadband magnetoelectirc sensor that overcomes many of the traditional problems. Generally, laminate composites have a higher ME voltage coefficient than sintered composites but exhibit limited to narrow bandwidth in terms of magnetic DC bias under the fixed AC magnetic field. This limits their ability to be utilized for an AC magnetic field sensing, which desires a flat ME response over a wide DC magnetic bias range.

Our research was guided by the fact that ME response in laminates was dependent on the geometry fabricated by using PZNT and Metglas layers, as shown in Fig. III.1. It was interesting to find that by changing the structure from "unimorph" type to "sandwich" type and from square shape to disk, the maximum in ME coefficient was shifted by more than 2 times (355 Oe shift).

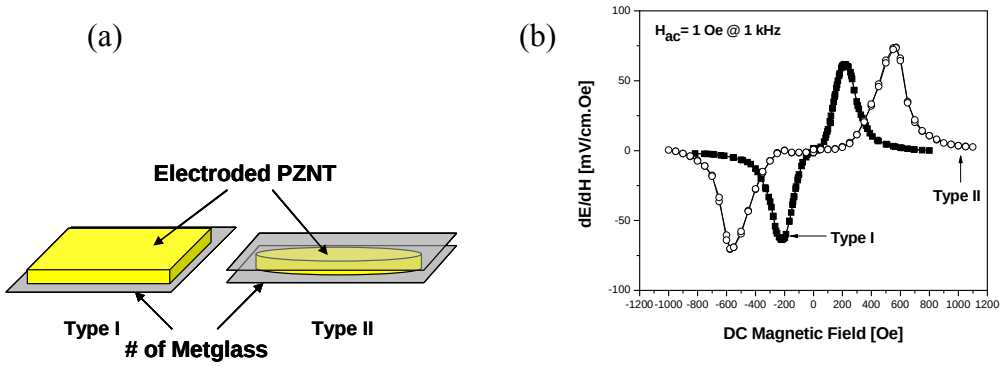

Fig.III.1. (a) Schematic diagrams of prepared samples: type I – 15.5×15.5 mm^2 PZNT plate with one side-attached Metglas and type II – 10.2 mm diameter PZNT disk with both side-attached Metglas, (b) Magnetoelectric output voltage as a function of DC magnetic field.

Based on these phenomena, some interesting observations can be made as following: (i) How can the two configurations be combined such that the ME coefficients are at maximum magnitude over the DC bias range of 215 Oe to 570 Oe?, (ii) What is the effect of stacking configurations on the maximum position of ME?, and (iii) What is the effect of interface area on ME coefficient?.

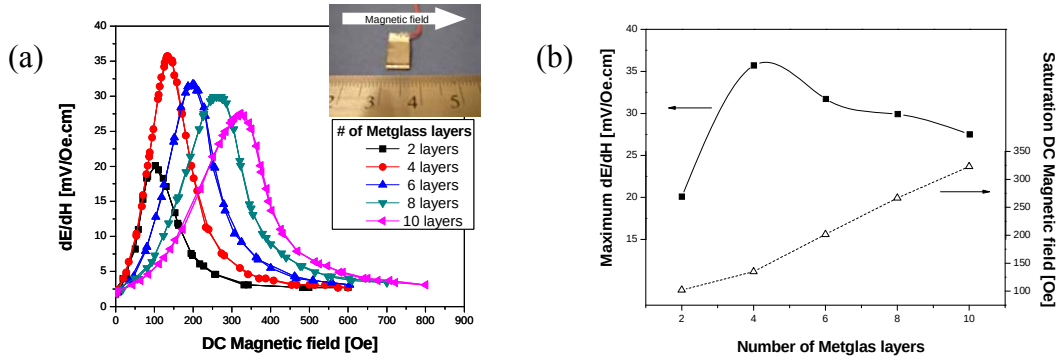

Fig.III. 2. Maximum ME coefficient and saturation DC magnetic field as a function of the number of Metglas layers on PZNT. All measurements were conducted under H_{ac}= 1 Oe and frequency of 1 kHz.

In order to investigate the role of the number of Metglas layers on the ME response, unimorph configuration was selected and 2-layers of Metglas with dimensions of 7×9 mm^2 were incrementally stacked on the PZNT plate of 7×15 mm^2. Figure III.2 shows the

variation of ME output voltage as a function of the number of Metglas layers and applied DC magnetic field. The composite with 4-layers of Metglas exhibited maximum magnitude of the ME coefficient. With further increase in the number of Metglas layers, the ME output steadily decreases. The optimum magnitude of magnetic DC bias (saturation DC magnetic field for magnetostriction coefficient) was found to increase with increase in the number of Metglas layers. It means that it is possible to control the ME output value and saturation point by changing the number of Metglas layers.

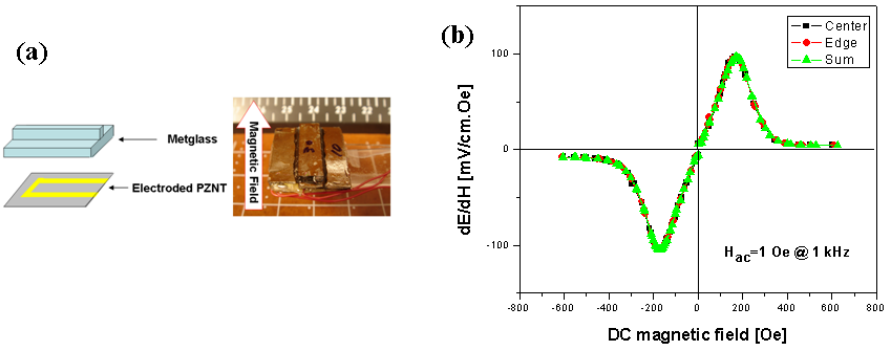

Fig. III.3. (a) Schematic representation of sample preparation with pyramid Metglas structure on separated electrodes. (b) Magnetoelectric output voltage as a function of applied DC magnetic field.

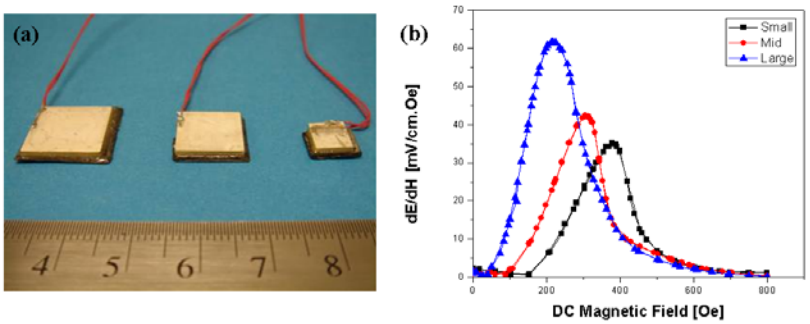

Fig. III.4. ME output voltage variation as a function of DC magnetic field for various dimensions. PZNT plates with different planar dimensions (15.5×15.5, 12.5×12.5, and 8×8 mm^2), but same thickness of 1 mm were used in this experiment. All ME measurements were conducted under H_{ac}= 1 Oe at 1 kHz.

In order to gain more information into the elastic coupling processes of unimorph configuration, a sectioned electrode pattern was designed on a PZNT plate of 15.5×15.5 mm^2. The electrode pattern on top of the PZNT plate is divided in two parts, a stripe is in between the "U" structure. The gap between the two sections was of the order of 1 mm. Ten-layered Metglas was attached on PZNT covering the whole surface area. In the center, on top of the stripe electrode, the number of Metglas layers was increased to thirty layers as shown in Fig. III.3. The ME coefficients were measured from the two sections separately, and then the combined response from the two sections was measured. Although locally different ME output behavior was expected from each section because of the difference in number of Metglas layers, the magnitudes of the ME coefficient and the saturation DC magnetic field were found to be identical from both sections. This indicates that average strain distribution is homogeneous, even though locally different strains are generated. Thus, it is important to have a larger physical separation in order to achieve differences between the peak positions of ME coefficient from two separated sections.

Figure III.4 shows the ME behavior as a function of DC magnetic field for three different samples. It was found that as the planar area of composites decreases, the ME voltage coefficient decreases, while the saturation DC magnetic field increases. Thus, the ME coefficient and saturation DC magnetic field exhibit inverse behaviors with increasing planar area. In other words, when the planar geometry is large, the ME coefficient is also large at smaller magnetic DC bias.

We realized a new geometrical structure is required to achieve the individual response from separate sections of composite. The composite design was guided by the above results: (i) different dimensions resulted in different peak positions with respect to magnetic DC bias, and (ii) physical separation between the Metglas layers was necessary to achieve a difference in the peak positions of the ME coefficient. Therefore, we incorporated these two factors by designing a dimensionally gradient composite with separate Metglas sections, as shown in Fig. III.5 (a).

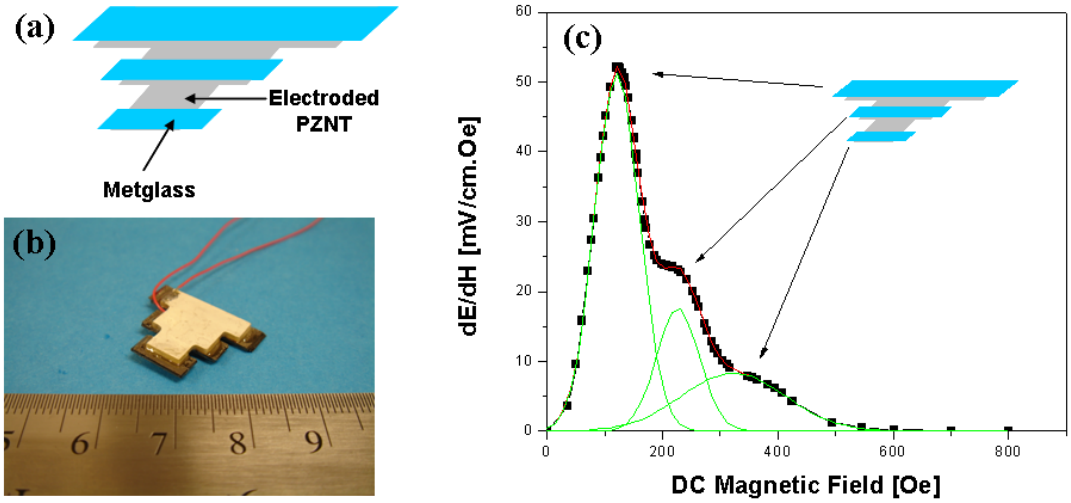

Fig. III.5. (a) Schematic structure of the dimensionally gradient sample, (b) Picture of the fabricated sample: 20-layers of Metglas was attached on each rectangular secction, (b) ME coefficient of the dimensionally gradient sample under H_{ac}= 1 Oe at 1 kHz.

The dimensions of the PZNT plate in each section were as follows: 15.5×5, 10.6×5.5, and 6.2×5 mm^2 (width of about 5 mm was reduced per 5 mm length) as shown in Fig. III.5(b). The thickness of the plate was 1 mm. On this structure, 20-layers of Metglas with proportional surface area were attached, where each Metglas section was separated from each other by 1.5 mm. Figure III.5(c) shows the measured ME response of this composite structure. Interestingly, the total ME response of the structure was in combination of the three individual effects, as shown by the peak fitting: three-typical components were found in the same specimen. As the planar dimension of composite decreases, the saturation magnetic field increases in providing three separate peaks from three different sections. The larger composite section exhibits a higher ME coefficient at smaller magnetic DC bias, in agreement with our result in Fig. III.4.

All results lead us to an important conclusion that a high magnitude and saturation point of ME coefficient can be controlled by composite structure having separated sections, dimensions of composite, and number of Metglas layers on a PZNT planar area. Based on this conclusion, we tested and demonstrated the broadband magnetoelectric

sensor. This result is important to realize different peak positions of the ME coefficient from different sections.

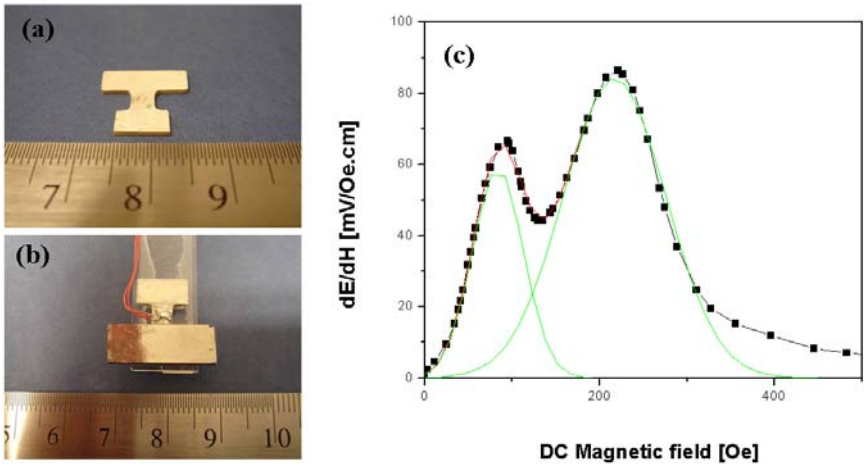

Fig. III.6. (a) Machined and electroded H-shaped PZNT plate, (b) Metglas-attached on the PZNT on both rectangular sections, (c) Broadband ME behavior of the H-shaped laminate.

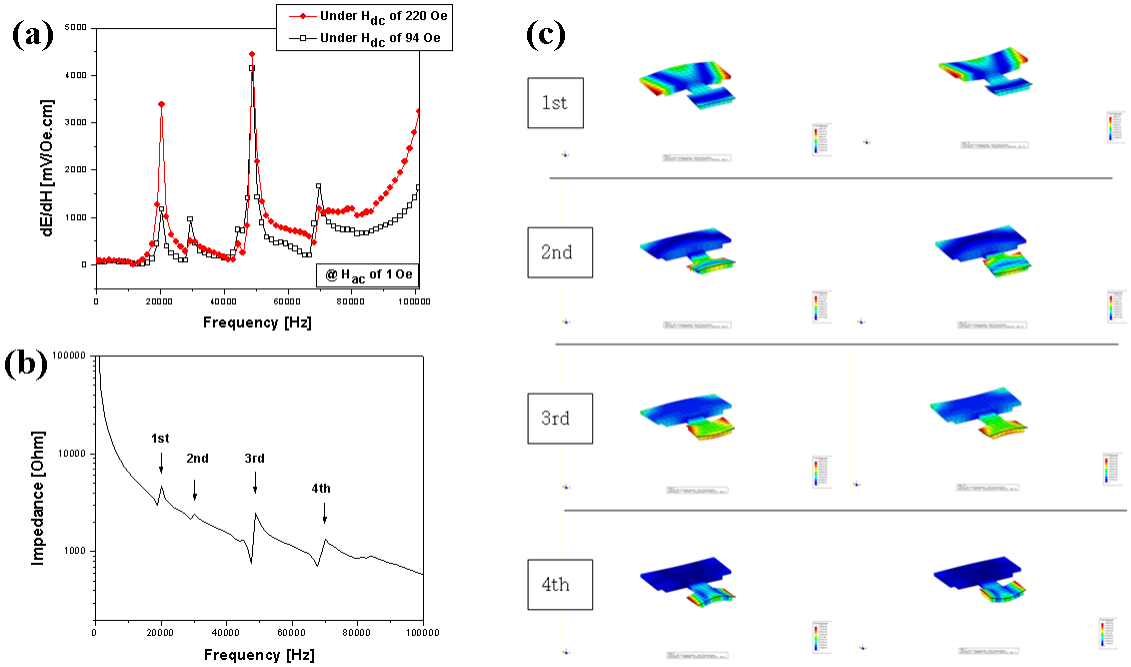

Fig. III.7. Frequency dependence of the ME coefficient for broadband laminate composite. (a) Measurements were conducted under H_{ac}= 1 Oe and H_{dc}= 94 and 220 Oe, (b) Resonance analysis-Impedance spectrum, (c) FEM analysis of bending resonance modes.

An asymmetric H shape PZNT plate was fabricated with the dimensions shown in Fig. III.6(a) (15.2×5.3 and 8.5×5 mm^2 areas were connected with the bridge of 4×5 mm^2) in order to enhance physical separation. In this design, the bridge connecting two different dimensions of laminate composites will lead to two separate responses. On this PZNT plate, 4-layers of Metglas was attached for the smaller area and 30-layers of Metglas was attached on the larger area. It should be noted here that smaller dimensions leads to smaller ME coefficient, but smaller number of Metglas layers leads to larger ME

coefficient. Thus, a compromise between the two opposing effects was calculated to be in the range equivalent to that of the large composite with 30-layered Metglas. Figure III.6(b) shows the picture of the fabricated composite. Figure III.6(c) shows the measured the ME response from this composite structure. The first peak of ME coefficient was found at 94 Oe associated with that of the 4-layered Metglas on a smaller piezoelectric surface area. The second peak of the ME coefficient was found at 220 Oe resulting from the 30-layered Metglas on the larger piezoelectric area. There is a slight drop in the magnitude of the ME coefficient between the two peaks, which reflects a mismatch in tailoring the dimensions of two sections. By further adjusting the dimensions, it is possible to bring the two peaks closer to each other and achieve almost a square wave response. However, the results of this figure clearly demonstrate the idea in designing the broadband magnetoelectric sensor.

Figure III.7(a) shows the frequency dependence of the ME coefficient for broadband composite in the range of 40 to 10^5 Hz. Measurement was conducted at H_{ac}= 1 Oe under applied DC magnetic fields of 94 and 220 Oe. The peaks in this figure correspond to electromechanical resonances occurring at 20, 29, 49, and 70 kHz. It is interesting to note that regardless of the applied DC magnetic field in the range of 94 – 220 Oe, the broadband ME sensor showed similar range of ME output voltage, ~4 V/cm.Oe, at 49 kHz. The maximum ME output was 4.5 V/cm.Oe under the conditions of H_{ac}=1 Oe at 49 kHz and H_{DC} = 220 Oe. In order to find the electromechanical resonance modes of PZNT plate – Metglas laminate, an FEM analysis was conducted using ATILA. Figure III.7(b) shows the impedance spectrum for H-shaped broadband laminate. The impedance spectrum was found to exhibit resonance peaks at the same position as that observed in the ME measurements as a function of frequency. This further indicates that all the peaks were correlated to electromechanical resonance modes. Figure III.7(c) shows the bending oscillation modes for the four resonances pointed in the impedance spectrum. The first mode at 20 kHz was found to be from bending of the large rectangular section in the H-laminate (Fig. III.7(c)-1st). The second mode at 29 kHz was found to be from the bending of bridge structure joining the two rectangular sections (Fig. III.7(c)-2nd). The output voltages from the 2nd mode were relatively low, which could be associated to the small deformation occurring in the bridge. The third mode at 49 kHz was related to combined bending response from the bridge and the small rectangular section of the composite (Fig. III.7(c)-3rd). This mode generated the highest output voltages as shown in Fig. III.7(a). The fourth mode at 70 kHz was found to be related to the bending of the small rectangular section of composite (Fig. III.7 (c)-4th). The results indicate that the third resonance mode at 49 kHz is a combination of the second mode occurring at 29 kHz and the fourth mode occurring at 70 kHz and leads to larger displacements in the structure, resulting in a higher ME coefficient. These results further provide the insight in designing a composite structure that could provide large ME coefficient over a wide frequency range.

Figure III.8 shows the sensitivity measurement of the broadband ME laminate to the small DC magnetic field variations under 49 kHz using L-T mode. These measurements were performed under H_{ac} = 0.1 Oe. Based on these resonant conditions, first a small dc magnetic field of 10 mOe was applied to the specimen. The ME voltage induced by step-like changes with a small dc bias of 10 mOe (1 μTesla) was measured using a time

domain capture mode, as shown in Fig. III.8(a). Clear responses in ME voltage per steps can easily sense 1 μTesla value of the small dc bias.

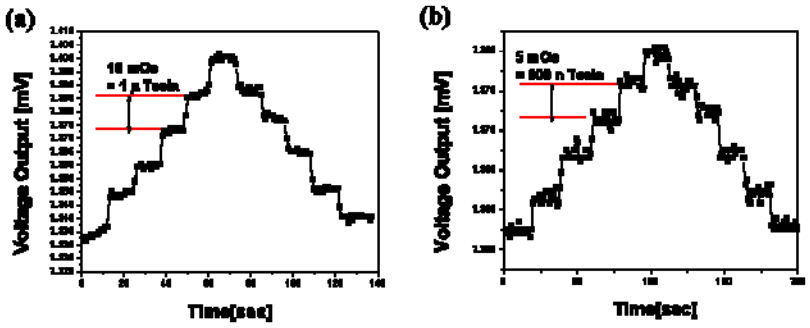

Fig. III.8. Sensitivity of small DC magnetic field for the L-T laminate under a constant H_{ac} =0.1 Oe at *f*= 49 kHz: (a) 1 μTesla and (b) 500 nTesla dc magnetic fields per steps.

Next, we reduced the applyied dc magnetic field to 5 mOe. The voltage output induced by steplike changes with small dc bias of 5 mOe (500 nTesla) was measured, as shown in Fig. III.8(b). Inspection of the data reveals rapid and visible responses in the voltage induced across the piezoelectric layers in response to ΔH_{dc}. This ME laminate can detect 500 nTesla value of H_{dc}. This sensitivity was attributed to the effective electromechanical resonance modes of the asymmetric H-shaped structure in the laminate at 49 kHz.

IV. Wideband sensor with Multi-layered Structure

We clearly demonstrated the idea in designing the broadband magnetoelectric sensor. However, there was still a problem to be solved. The response at electromechanical resonance (EMR) frequency is 10 – 100 times higher than in the low frequency regime. Further, the ME composites exhibit narrow and sharp peak behaviors at EMR frequency. If an operating frequency is not exactly at EMR, the response would be weak. In magnetic field sensor applications, an ideal scenario would be to achieve the EMR frequency below 1 kHz and increase both the frequency and magnetic DC bias range in which the ME coefficient almost remains flat. This is the motivation behind our research, and we present our progress is design and fabrication of wideband magnetoelectric composites in this section.

To achieve wideband AC magnetic field sensing, some conditions should be met: (i) generating multiple resonance modes, (ii) merging these resonance peaks, (iii) moving the EMR to the range of 1 kHz. A bimorph-type asymmetric H-shaped piezoelectric ceramic was employed to generate various resonance modes. Using the tip loading method resonance frequency was reduced further.

Figure IV.1(a) shows the schematic of asymmetric H-shaped bimorph. This exhibited multiple resonances below 100 kHz as shown in Fig. IV.1(b). The impedance and phase spectrums indicated resonance peaks at 10.09, 13.08, 23.32, 33.81, 43.05, 58.54, and 82.26 kHz. For comparison, we have analyzed the resonance spectrum of H-shaped ceramic plate of similar dimensions which showed only three EMR peaks at 40, 70, and 94 kHz. The presence of these additional peaks allowed us to merge them in the desired operating range resulting in the wide band response.

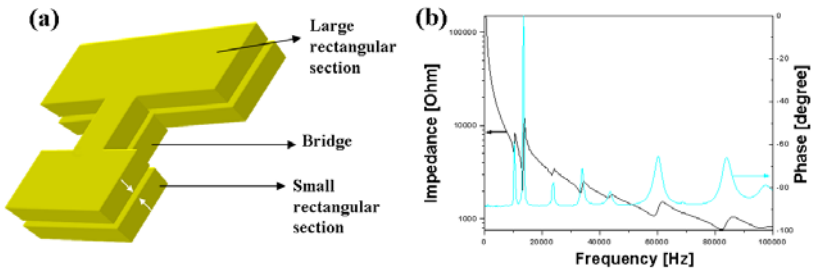

Fig. IV.1. (a) Schematic diagram of asymmetric H-shaped bimorph with opposite poling directions in piezoelectric layers. The dimensions of two rectangular sections were 15.5×5 and 9.5×5 mm^2 connected by a bridge of dimension 4×5 mm^2. The thickness of each layer was 500 μm. (b) Impedance and phase spectrum for the asymmetric H-shaped bimorph.

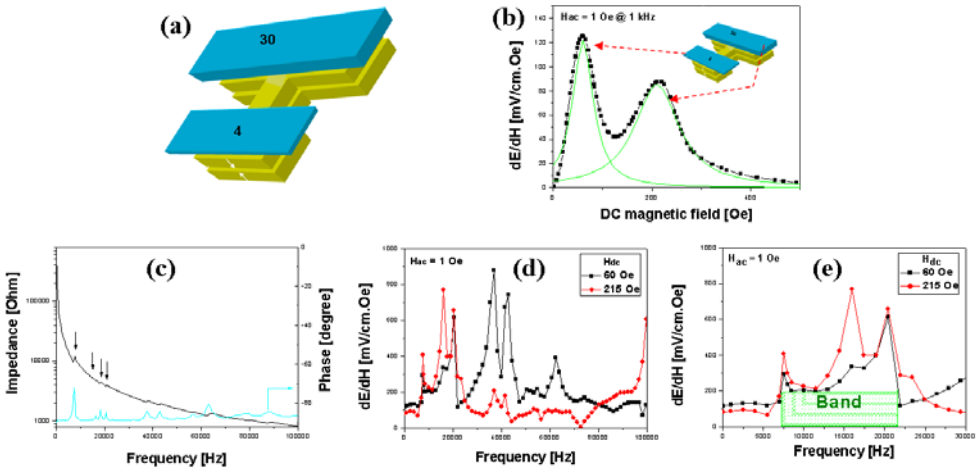

Fig. IV.2. (a) Inset: Schematic diagram of Metglas attached to the bimorph. Four layers of Metglas of area 15×7 mm^2 was attached on smaller rectangular section while thirty layers of Metglas of area 20×7 mm^2 was attached on the larger rectangular section. (b) ME sensitivity as a function of magnetic DC bias at frequency of 1 kHz and applied AC magnetic field of H_{ac}= 1 Oe, (c) Impedance and phase spectrums as a function of frequency, (d) ME coefficient as a function of frequency until 100 kHz, and (e) ME coefficient as a function of frequency until 30 kHz.

On this PZNT bimorph, four layers of Metglas with an area of 15×7 mm^2 was attached at the smaller section and thirty layers of Metglas, with an area of 20×7 mm^2 was attached at the larger section, as shown in Fig. IV.2(a). By adjusting the ratio of Metglas layers to the area of the piezoelectric rectangular sections an average response can be obtained from the H-shaped structure. Figure IV.2(b) shows the measured ME response from bimorph composite structure as a function of magnetic DC bias at the frequency of 1 kHz with 1 Oe applied AC field. The peak at 60 Oe was associated with the four-layered Metglas section on the smaller piezoelectric surface area. The second peak of the ME coefficient at 215 Oe is associated with the thirty-layered Metglas section on the larger piezoelectric area. The impedance and phase angle spectrum for this laminate is shown in Fig. IV.2(c). After Metglas was attached on the PZNT plate, the intensity of resonances became smaller which can be explained by the dampening effect and the position of peaks shifted towards lower frequencies, as shown in Fig. IV.2(c). The weight of Metglas on the PZNT plates also brought the four peaks initially found at 7.3, 16.3, 18.3, and 20.5 kHz originated from 10.09, 13.08, 23.32, 33.81, and 43.05 kHz in Fig. IV.1(b), but closer to each other. More specifically, the peak at 7.3 kHz in Fig.

IV.2(c) was combined with the peaks of 10.09 and 13.08 kHz in Fig. IV.1(b). As a result, a wide-band was formed in the frequency range of 7 – 22 kHz, as shown in Fig. IV.2 (d) and (e). This band comprises of peaks in the ME coefficient at 7.5 and 20.43 kHz at the magnetic DC bias of 60 Oe. Under the magnetic DC bias of 215 Oe, the peaks occur at 7.5, 15.95, and 20.43 kHz. This indicates that the peak at 15.95 kHz was related to the magneto-mechanical coupling and not to the electromechanical coupling. The ME sensitivity of the sensor in this band was measured to be higher than 200 mV/cm.Oe independent of the magnitude of applied magnetic DC bias. Furthermore, this wideband frequency response can be shifted using tip masses at the ends of the sensor. These results are quite promising for practical applications such as current probe and magnetic field sensing.

V. Multilayer Co-fired ME Composite

We have successfully fabricated a laminate composite which has a 3-layered structure with piezoelectric/magnetostrictive/piezoelectric using tape casting technique. The compositions of $0.2Pb(Zn_{1/3}Nb_{1/3})$-$0.8Pb(Zr_{0.5}Ti_{0.5})O_3$ [PZNT] and $(Ni_{0.6}Cu_{0.2}Zn_{0.2})Fe_2O_4$ [NCZF] were selected for sintering. PZNT and NCZF powders were calcined at 850° C. The powders were mixed with the binder system and solvent for tape casting. For the PZNT slurry, 50 wt% of the binder system with respect to the PZNT powder was added. For the NCZF slurry, 65 wt% of the binder system with respect to the NCZF powder was added. PZNT and NCZF slurries were tape-casted with 250 μm height of doctor blade, as shown in Fig. V.1 (a).

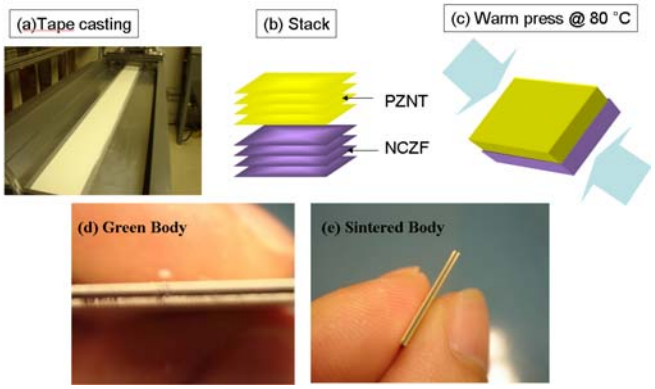

Fig. V.1. Tape casting processing: (a) casted tape, (b) stacking, (c) warm pressing, (d) green body, (e) sintered sample.

After tape casting, the tape was dried for 24 hours. The green sheets were cut, laminated, and pressed under 5 MPa pressure at 80°C, as shown in Figs. V.1 (b) and (c). Consequently, the laminated green body was formed as shown in Fig. V.1 (d). These green bodies were baked at 400°C for 4 hrs with a heating rate of 0.3°C/min to remove organic binders. Subsequently, sintering was conducted at 930°C for 4 hrs with a heating rate of 1°C/min. After the binder burnout and sintering processes, the laminated composite was successfully co-fired without any cracks or delaminations, as shown in Fig. V.1 (e).

Figure V.2(a) shows the ME coefficient of laminate composite as a function of DC magnetic field in longitudinal-transverse (L-T) mode. It shows the peak value of 82 mV/cm.Oe at H_{dc} = 67 Oe and H_{ac} = 1 Oe at 1 kHz. Prior reports on sintered ME

composites based on NZF or NCZF show the peak ME value at a DC magnetic field of around 400 Oe; however, in this case the peak ME value was found to occur at 67 Oe. This low saturation in ME composites could be related to the changes in the coercivity of the composite. The magnetization of laminate composite as a function of magnetic field was measured by VSM using longitudinal direction (L-mode), as shown in Fig. V.2(b).

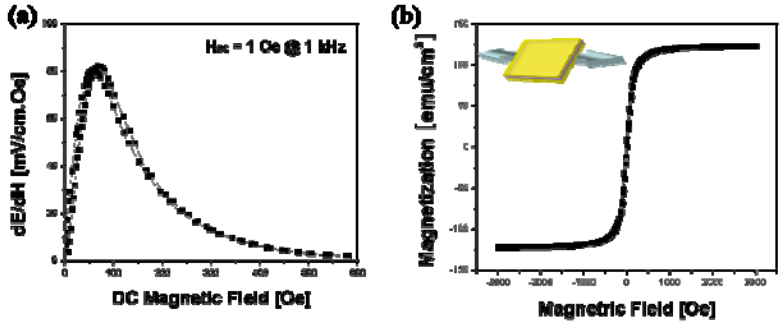

Fig. V.2. (a) ME coefficient as a function of DC magnetic field under H_{ac} =1 Oe at 1 kHz, (b) Magnetization as a function of magnetic field. Measurement was conducted at room temperature using longitudinal mode.

The coercive magnetic field (H_c) and remanent magnetization (M_r) were found to be 16 Oe and 11.2 emu/cm^3 respectively. The saturation magnetization was 122 emu/cm^3. The magnetic domain was switched under low magnetic field representing ferrimagnetic properties. This result indicates why the ME behavior was saturated at a low DC magnetic field. The coercivity and saturation behaviors at the low magnetic field resulted in high ME sensitivity.

Figure V.3(a) shows the sensitivity of L-T ME laminate to the small DC magnetic field variations at 1 kHz. The voltage induced by step-like changes under the small dc bias of 10 mOe (1 μTesla) in the range of 0 - 0.05 Oe (H_{dc}) was measured using time domain capture mode. These measurements were performed under H_{ac} = 1 Oe. Inspection of the data reveals rapid and stable responses in the voltage induced across the piezoelectric layers in response to ΔH_{dc}. This ME laminate composite was found to detect 1 μT value of H_{dc}, which is an extremely good performance for a 3-layered structure.

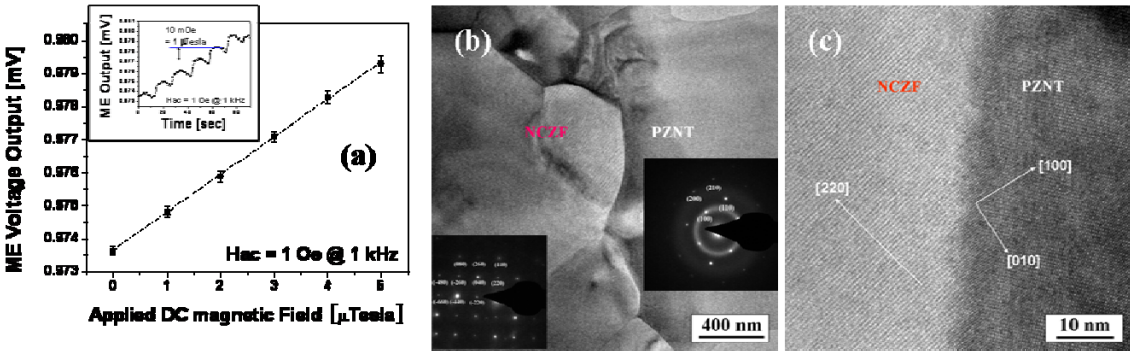

Fig.V.3.(a) Sensitivity limit of small DC magnetic field for the L-T laminate under a constant H_{ac} =1 Oe at *f*= 1 kHz, (b) TEM and SAED images, (c) High resolution TEM images.

This sensitivity was attributed to the effectiveness of elastic coupling due to defect-free interfaces in laminate structure, as shown in Fig. V.3 (b) and (c). (HR-TEM image shows the perfect interfaces without any defects). Fabrication of co-fired laminate composites with high magnetic-field sensitivity will lead to their wide scale application.

VI. Co-fired 3-1 Composite Structure

The 3-1 composite was successfully synthesized using a co-firing technique by adjusting thermal expansion behaviors. $0.2Pb(Zn_{1/3}Nb_{2/3})$-$0.8Pb(Zr_{0.5}Ti_{0.5})_{1-x}O_3$ [PZNT] and $(Ni_{0.6}Cu_{0.2}Zn_{0.2})Fe_2O_3$ [NCZF] powders were chosen as two phase materials. Various-types of vertical 3-1 composites were fabricated using thermoplastic properties of tape casting approach. Subsequent sintering was conducted at 930°C for 4 h with a heating rate of 1°C/min.

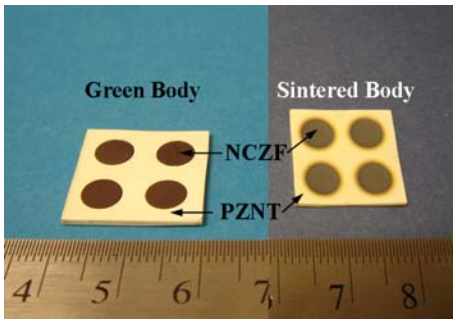

Fig. VI.1. Green and sintered bodies of 3-1 composites: Green body - 20×20×1 mm^3, Sintered body – 16.5×16.5×0.8 mm^3.

Figure VI.1 shows the green (left) and sintered (right) bodies of vertical 3-1 composites which were composed of NCZF (Pillar) and PZNT (Matrix) materials. After binder burnout at 400°C for 4 h with a heating rate of 0.3°C/min to remove organic binders, co-firing was successfully conducted at 930°C without any delaminations and cracks. Electrodes were printed on only the PZNT area; and then the specimens were poled at 4 kV/mm. Thereafter, the ME properties of these composites were measured as a function of dc magnetic field under the condition of H_{ac} = 1 Oe at 1 kHz using L-T mode. The composite having a single dot of NCZF in the PZNT matrix exhibited the maximum magnitude of the ME coefficient of 7 mV/cm.Oe at H_{dc} = 340 Oe while the composite having 4 dots of NCZF in the PZNT matrix showed 15 mV/cm.Oe at H_{dc} = 340 Oe, as shown in Fig. VI.2. When the number of dots increased in the 3-1 composites, ME output voltage also increased. However, the saturation magnetic field was not changed even though the number of dots increased. The ME coefficients of 3-1 composite exhibited relatively low values.

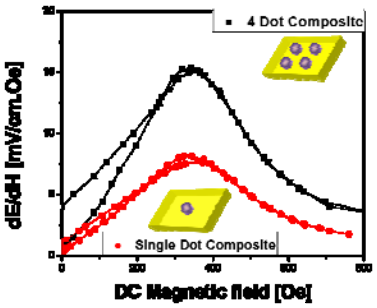

Fig. VI.2. Magnetoelectric output voltage as a function of DC magnetic field of single-dot and 4-dot composites.

VII. 2-1-2 connectivity Sensors (New design & Analytical Modeling)

We synthesized a three phase 2-1-2 composite by co-firing NCZF pillars in the PZNT matrix and by laminating with Metglas layers. Magnetostrictive Metglas foils were laminated on top and bottom of the PZNT layer with embedded NCZF pillars, changing the overall connectivity to 2-1-2, where PZNT is connected two dimensionally, NCZF is

connected one dimensionally, and Metglas is connected in two dimensions. In order to analyze the performance of this composite, a systematic study was conducted to evaluate the effect of each additional layer and the strain coupling occurring between ferrite and Metglas. Figure VII.1(a) shows the schematic of unimorph and bimorph configurations for the 2-1-2 composite consisting of four-layers of Metglas on each side (thickness of one layer of Metglas = 25 μm).

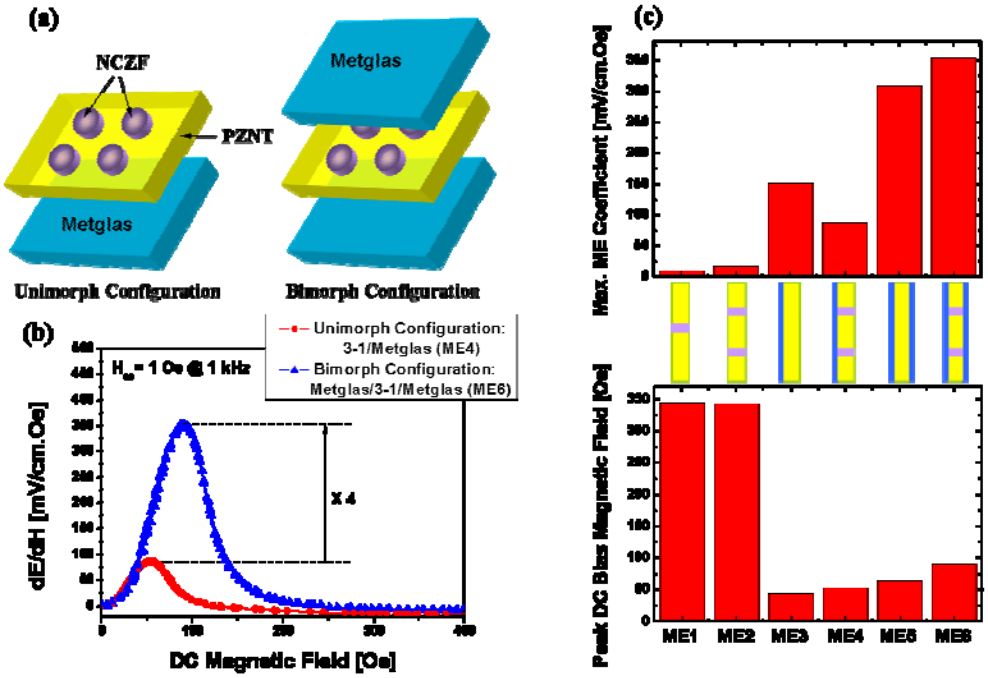

Fig. VII.1. (a) Schematic diagrams of unimorph and bimorph configurations with intermediate layer of 3-1 laminate composite consisting of 4-layered Metglas, (b) ME coefficient of 3-1 composite depending on the laminations: 3-1/Metglas (ME4) and Metglas/3-1/Metglas (ME6), (c) Histogram plots of the maximum magnetoelectric coefficient and the optimum DC bias magnetic field as a function of the six different composite structures .

Figure VII.1(b) shows the variation of the ME coefficient as a function of magnetic DC bias for both unimorph and bimorph configurations. For the unimorph configuration, the peak ME coefficient was found to be of the order of 86 mV/cm.Oe at H_{dc} = 52.8 Oe (ME4). For the bimorph configuration, the magnitude of ME coefficient increased to 352.5 mV/cm.Oe at H_{dc} = 89.5 Oe (ME6), as shown in Fig. VII.1(b). There was a 4X increase in the ME coefficient by attaching the Metglas layers on both sides of the PZNT plate. This is quite an interesting result, and understanding this behavior requires information on 2-2 laminate composites with identical configuration but without any embedded ferrite pillars. Figure VII.1(c) compares the magnitude of maximum ME coefficient and optimum magnitude of the magnetic DC bias for all six different composites investigated in our group. Based on these composites, we tried to figure out the origin of the ME enhancement in terms of semiempirical models.

Using a simple product property relationship, we can estimate the magnitude of the ME coefficient for the composite as:

$$ME = {}^{m}v\,(dS/dH)_{ferrite}(1 - {}^{m}v)\,(g_{31}.C_{31})_{piezoelectric} \qquad \text{(VII.1)}$$

where ^{m}v is the volume fraction of ferrite, S is the strain, H is the applied magnetic field, g_{31} is the piezoelectric strain constant, and C_{31} is the elastic stiffness. Using Eq.(VII.1) it can be shown that:

$$ME2 / ME1 = 2.98\,(dS'/dS)_{ferrite} = 2.98\eta \qquad \text{(VII.2)}$$

where S' is the average strain in the composite with four pillars and η is the efficiency factor. The diameter of the single ferrite pillar in the sintered body was taken to be 5.2 mm and the total dimension of the sintered sample was 16.5×16.5×0.8 mm^3. The relationship shown in Eq.(VII.2) is reasonable given the fact that saturation in the magnetoelectric coefficient occurs at a similar value of magnetic DC bias. The estimation of η requires information on variation of elastic strain fields within the composite which is quite complex. However, using the approximation that sample is homogeneous and uniform, we can write for the average strain in ME2 composite as:

$$dS' = \frac{^{m}v}{V}\sum_{i}^{N_i}\frac{1}{^{m}v}\int dr_i\, S'(r_i) \qquad \text{(VII.3)}$$

where V is the total volume such that $N_i = {}^{m}v/V$. Further, assuming that S_i is the average value of integral in the region i, then integral can be written as:

$$dS' = \frac{^{m}v}{V}\sum_{i}^{N_i} dS_i \qquad \text{(VII.4)}$$

Dividing the sample into four quadrants, and noticing that strain generated in each pillar in response to applied magnetic field will be constrained by at least two nearest neighbors. Thus, the strain magnitude for each pillar in the four regions can be reasonably assumed to be half of that for the single pillar structure with no neighbors, i.e. dS/2. Substituting, this value of strain in Eq.(VII.4) and taking the summation over four regions, the efficiency factor can be determined to be as:

$$\eta = (dS'/dS)_{ferrite} = 2.\ {}^{m}v'/V = 0.624 \qquad \text{(VII.5)}$$

where $^{m}v'$ is the volume fraction of ferrite in 3-1 composite with four pillars. Substituting the value for the efficiency factor from Eq.(VII.5) in Eq.(VII.2), the ratio ME2/ME1 can be determined to be 1.859. Experimentally, the ratio was found to be 1.89.

The magnetoelectric model originally proposed by Srinivasan et al. for the bilayer and multilayers composites has been widely utilized. According to this model, by doubling the volume of magnetostrictive layer (bimorph vs. unimorph, or ME5 vs. ME3), the increase in the magnitude of the ME coefficient can be given as:

$$ME5/ME3 = 2\left[\frac{1}{1+\dfrac{t_{Met}\left(\left({}^{p}s_{11}+{}^{p}s_{12}\right){}^{p}\varepsilon_{33}^{T}-2\,{}^{p}d_{31}{}^{2}\right)}{t_{PZNT}\left({}^{m}s_{11}+{}^{m}s_{12}\right){}^{p}\varepsilon_{33}^{T}+t_{Met}\left(\left({}^{p}s_{11}+{}^{p}s_{12}\right)\varepsilon_{33}^{T}-2\,{}^{p}d_{31}{}^{2}\right)}}\right] \qquad \text{(VII.6)}$$

where t is the thickness of respective layers, s is elastic compliance, d is piezoelectric constant, ε^{T} is permittivity at constant stress, subscript Met stands for Metglas, and superscripts m and p stand for magnetostrictive and piezoelectric phases. The magnitude of the term in the square brackets can be estimated to be in the vicinity of ~0.93 by assuming following conditions: $^{m}s_{11} = {}^{p}s_{11}$, $^{m}s_{12} = {}^{p}s_{12}$, $t_{PZNT} = 8\ t_{Met}$, $^{p}d_{31} = 100$ pC/N, and $\varepsilon_{33}{}^{T}/\varepsilon_{o} = 1000$. This magnitude is close to that observed by the experiment. In practice, the magnitude of elastic compliance for the amorphous magnetostrictive phase and the

crystalline piezoelectric phase is quite different. Thus, Eq.(VII.6) could be approximated as:

$$ME5 \approx 2\ ME3 \qquad \text{(VII.7)}$$

In order to compute the magnitude of the ME coefficient for the ME4 composite, we conducted comparative analysis between ME3 and ME4 and make the following observations: (i) active volume of PZNT in ME3 is replaced by 4 NCZF pillars in ME4, (ii) peak ME coefficient occurs at a similar value of magnetic DC bias in both ME3 and ME4, and (iii) the magnetic DC bias corresponding to the peak in ME coefficient is far from that required for NCZF to saturate as seen by making comparison with ME1 and ME2. Thus, the contribution from NCZF pillars towards the ME response will be quite small as compared to that from Metglas layers. Since NCZF pillars are unclamped on the other side in unimorph configuration (ME4), any strain occurring through the deformation in radial direction will be relaxed. Thus, the only factor affecting the response of ME4 composite will be interaction between the Metglas layer and PZNT which directly correlates with the reduction in the volume of active piezoelectric layer and no contribution from the 3-1 (PZNT-NCZF) composite, given as:

$$ME4 = ME3\ (1- (4.^{m}v)/V\ ) - ME2 = 87.82\ \text{mV/cm.Oe} \qquad \text{(VII.8)}$$

This magnitude is quite close to that measured experimentally. The composite ME6 is modification of ME4 with bimorph structure consisting of Metglas layers on both sides of 3-1 composite. One would expect the magnitude of ME6 to be ~2 ME4 based on Eq.(VII.6), but the results show that it was ~4 ME4. The difference in the optimum magnetic DC bias for ME3 and ME4 composites was 9.7Oe while that for ME5 and ME6 was 26.8Oe. This increase in the magnitude of optimum magnetic DC bias can be correlated with the magnetic interaction between Metglas and NCZF which should contribute towards the enhanced strain in the PZNT layer. We believe this contributes towards the enhancement of the ME response. The models for 3-phase composites are not yet developed but we can approximate the contribution due to the ferrite pillars as ME2/ME1 given through Eq. (VII.2). Thus using Eq.(VII.8) and Eq.(VII.2), the magnetoelectric response for ME6 can be written as:

$$ME6 = [ME5\ (1- (4.^{m}v)/V\ ) - ME2] \times (ME2/ME1) \qquad \text{(VII.9)}$$

which can be calculated to be 370.7 mV/cm.Oe. The experimentally measured value for ME6 was 352.5 mV/cm.Oe. This difference might be related to the fact that the strain due to ferrite pillars is overestimated by the ratio ME2/ME1. These results clearly demonstrate the effectiveness of 2-1-2 composite structure.

Figure VII.2 shows the voltage output responses corresponding to a small applied DC magnetic field of 500 nTesla. This represents the sensitivity limit of current 2-1-2 ME laminate for detecting a small DC magnetic field under the operating condition of H_{ac} = 1 Oe at 1 kHz in L-T mode. The voltage induced by step-like changes of small DC bias of 5 mOe (500 nTesla) was measured. The output responses corresponding to the 500 nT value of small DC bias per step were clear without any overlaps of the standard deviations. It means the resolution of composite for the DC bias can be operated less than 500 nT value.

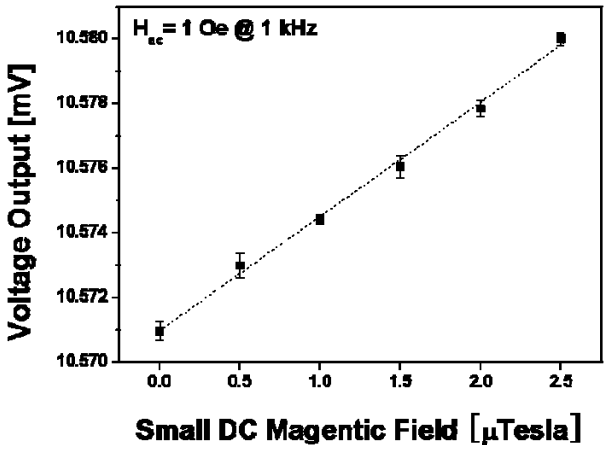

Fig. VII.2. Voltage output responses corresponding to an applying small DC magnetic field of 500 nTesla for the L-T laminate (ME 6) under a constant H_{ac} =1 Oe at *f*= 1 kHz.

Inspection of the data reveals visible changes in the voltage induced across the piezoelectric layers in response to varying ΔH_{dc} of 500nT. These results clearly demonstrate the effectiveness of 2-1-2 composite structure.

VIII. NanoTesla Sensitivity ME Composite using Active Tip-Mass

The high sensitivity ME composite with the maximum resolution of 5 nT was successfully achieved using Metglas / piezoelectric / carbon fiber / piezoelectric laminates with active tip mass. In order to maximize ME properties and to minimize magnetoelectrical degradations, we investigated (i) effect of the higher order bending modes, (ii) effect of the rigid clamping on the response of fixed – free cantilever beam, and (iii) effect of the active tip mass (ferromagnetic).

Piezoelectric stripes with dimensions of 60×20×0.6 mm^3 were selected as the base structure. The stripes themselves consisted of a carbon fiber substrate (C) bonded between two layers of PZT-5X45 (P). On top of the piezoelectric layer, a 100 μm-thick Metglas layer (M) was bonded (MPCP laminate). Four different configurations with varying tip masses were investigated. The initial configuration had no tip mass and therefore, acts as a reference for comparative analysis. The 2nd configuration had a 1 g "passive" or non-magnetic tip mass made from PZT ceramic. For the 3rd and 4th configuration, 1 g and 2 g "active" nickel (Ni) tip masses were utilized.

Figure VIII.1(a) shows the impedance vs. frequency behavior for the unclamped (free-free) and clamped (fixed-free) MPCP laminate. The rigid clamping resulted in sharp resonance behavior at low frequency and thus was used for further investigations. Figure VIII.1(b) shows the variation of magnetostriction and piezomagnetic coefficient of the MPCP laminate as a function of DC magnetic field (H_{dc}). The coefficients, λ_{11} and λ_{12} correspond to the in-plane magnetostriction coefficients measured parallel and perpendicular to applied H_{dc}. When H_{dc} was applied in longitudinal direction of the specimen, the Metglas elongated in the same direction by 28 ppm and contracted in the lateral direction by 22 ppm. The parameters q_{11} and q_{12} are in-plain piezomagnetic coefficients ($q_{ij}=d\lambda_{ij}/dH$). The maximum q_{11} and q_{12} were obtained at H_{dc}= 8 Oe with values of 1.08 and -0.75 ppm/Oe, respectively. Thus, low-field saturated ME behavior and high ME coefficient for MPCP laminate can be expected. The functional change of

piezomagentic coefficients has resemblance to the measured ME voltage coefficient. The peak in the ME coefficient of 394 mV/cm.Oe was achieved at the low DC bias field of H_{dc} = 7.7 Oe. Based on the measurement of impedance and phase angle the laminate was found to exhibit the first bending resonance at 54 Hz and the second bending resonance at 595 Hz.

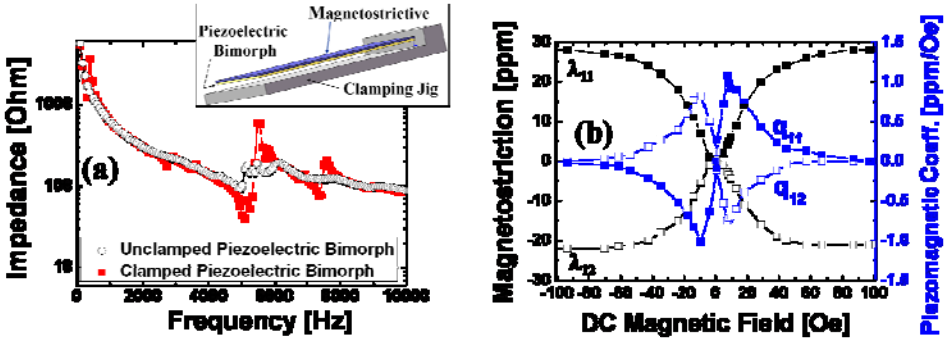

Fig. VIII.1. (a) Impedance spectrum of PCP laminate measured using impedance analyzer in unclamped and clamped (cantilever beam) configurations, Inset: CAD model of MPCP with clamping condition, (b) Magnetostriction and piezomagnetic coefficient for varying magnitude of DC magnetic field.

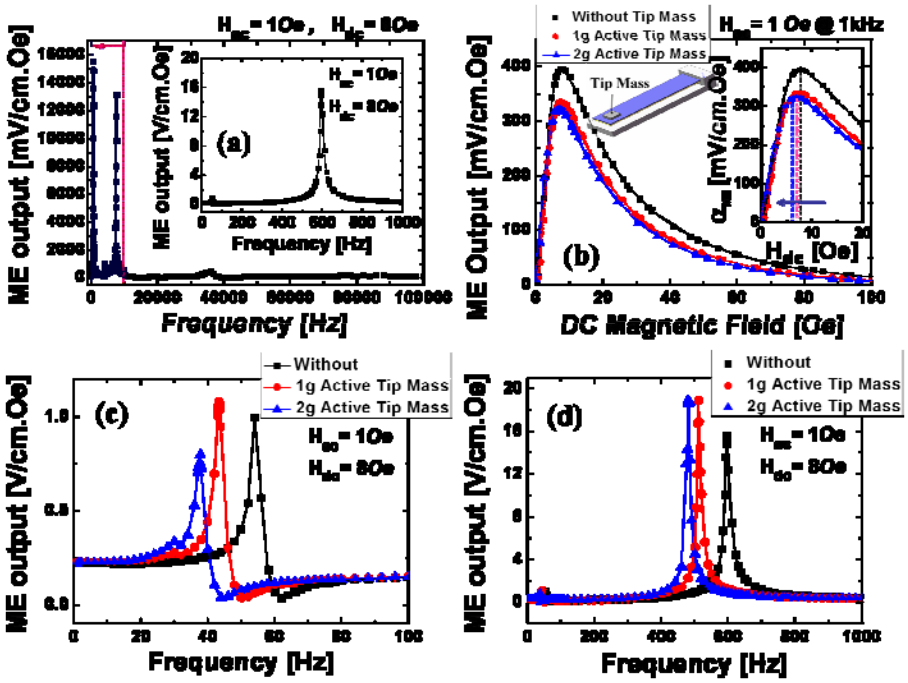

Figure VIII.2. (a) Measured ME output of MPCP laminate without tip mass as a function of excitation frequency with applied AC magnetic field of 1 Oe. The large magnitude of the first two bending modes can be clearly seen in the inset, (b) ME voltage output as a function of DC magnetic field under the condition of H_{ac}= 1 Oe at 1 kHz with multiple active tip mass configurations, (c) ME voltage output as a function of frequency around the first bending mode, (d) second bending mode for various tip mass configurations.

The ME response of laminate as a function of frequency was measured under the conditions of H_{ac}=1 Oe and H_{dc}=8 Oe, as shown in Fig. VIII.2(a). The maximum ME response of 15.5 and 13.1 V/cm.Oe was obtained at 595 and 7549 Hz. The first ME resonant peak occurred at 54 Hz with the magnitude of 1 V/cm.Oe. These strong ME

responses at low frequency were attributed to: (i) effective bending modes and (ii) effective clamping. The ME coefficients depending upon the active mass were measured as a function of the DC magnetic field under the constant condition of H_{ac}=1 Oe at f = 1 kHz, as shown in Fig. VIII.2(b). The peak ME value without tip mass was measured to be 394 mV/cm.Oe at 1 kHz. With 1g active tip mass, this magnitude was reduced to 333 mV/cm.Oe while with 2g active tip mass it was further decreased to 322 mV/cm.Oe. The ME peak position decreased from 7.7 to 7 Oe with increase in active tip mass from 0g to 2g. However, the traces of ME coefficients up to 4.5 Oe were identical as seen in Fig. VIII.2 (b). This indicates that ME responses for small bias would be similar regardless of tip mass.

The shift in EMR frequency depending upon the magnitude of active tip mass was quantified by impedance measurements. The first bending mode was found to occur at 54 Hz without tip mass, which decreased to 43 Hz on addition of 1g tip mass and further decreased to 37 Hz by adding 2g tip mass. The second bending mode at 595 Hz moved down to 511 Hz and 480 Hz with the addition of 1g and 2g tip masses, respectively. The ME behavior depending upon the magnitude of active tip mass was measured as a function of frequency under the constant conditions of H_{ac}= 1 Oe and H_{dc}= 8 Oe. The peak ME positions in Fig. VIII.2(c) were well matched to the EMR results. The ME output voltage coefficient of 1 V/cm.Oe at 54 Hz increased to 1.08 V/cm.Oe at 43 Hz with 1g tip mass, but decreased to 0.8 V/cm.Oe at 37 Hz with 2g tip mass, as shown in Fig. 2(c). For the second bending mode, the ME output voltage of 15.5 V/cm.Oe at 595 Hz increased to 19 V/cm.Oe (22%) for both 1g and 2g tip mass, as shown in Fig. VIII.2(d). For the first bending mode, the 1g active tip mass configuration exhibited the best ME output. For the second bending mode, both 1g and 2g active tip masses effectively increased the ME coefficient. These results clearly demonstrate that second bending mode can be effectively tuned without any severe drop in the ME output voltage by using the active tip mass. For comparison, a fourth configuration of MPCP laminate was fabricated with 1g non-active tip mass. In this case, the ME peak position increased from 7.7 to 8.3 Oe (~0.6 Oe), and the ME magnitude decreased by 14%. Both of these effects are undesirable. Furthermore, the initial slope of the ME curve was also decreased. The non-active tip mass leads to the ME coefficient degradation and reduction of the ME magnitude at resonance.

Using ATILA finite element method (FEM), the first bending mode for the MPCP laminate with 1g tip mass was calculated to be 51 Hz, which is slightly different from experimentally measured 43 Hz. The main reason for this difference was clamping. Since ideal clamping is not possible in an experimental setting, small variation is expected. A second bending mode for the structure was calculated to be 502 Hz. Two main analyses were conducted using ATILA: (i) stress along various directions (XX, YY, ZZ, XY, XZ, and YZ), and (ii) deformation along the length. The analyses are shown in Figs. VIII.3(a) and (b). In both figures, the x-axis represents the length of the MPCP laminate and the y-axis represents the shear stress distribution in the XY direction (left) and deformation (right). The MPCP laminate was symmetrical across the width (w); therefore, the stress and deformation along the length of the beam is reported at three sections w=0, w=1/4 and w=1/2. At the first bending mode in Fig. VIII.3(a), the stress levels are the highest only near the clamped end of the beam. Further, it can be noticed that the stress across the width was highest at w=0 and it decreases towards the center of

the beam, w=1/2. Figure VIII.3(b) shows the stress and deformation distribution of the MPCP laminate at the second bending mode. In this case, the highest deformation is seen at half the length of the ME laminate from at its free end. The second mode also produces two widely and highly stressed areas which are the main reason behind higher voltage output compared to the first mode.

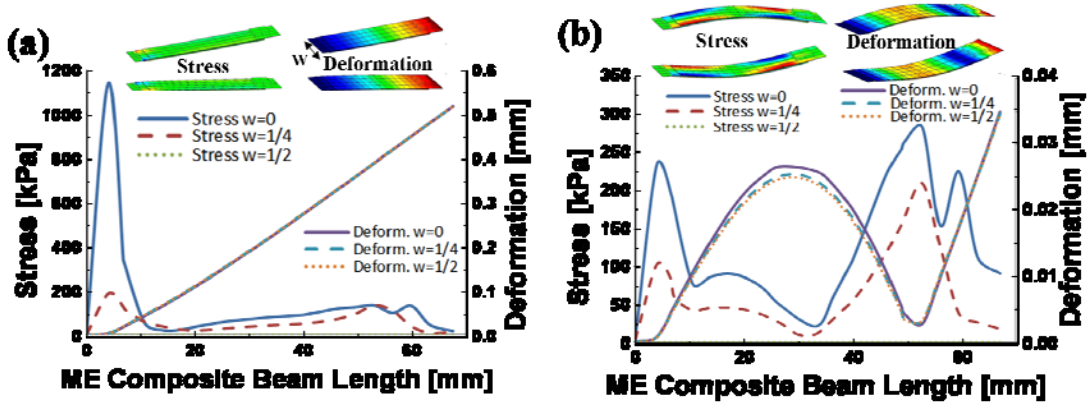

Figure VIII.3. Stress and deformation distribution along the length of the MPCP laminate with 1g active tip mass, (a) at the first bending mode and (b) at the second bending mode.

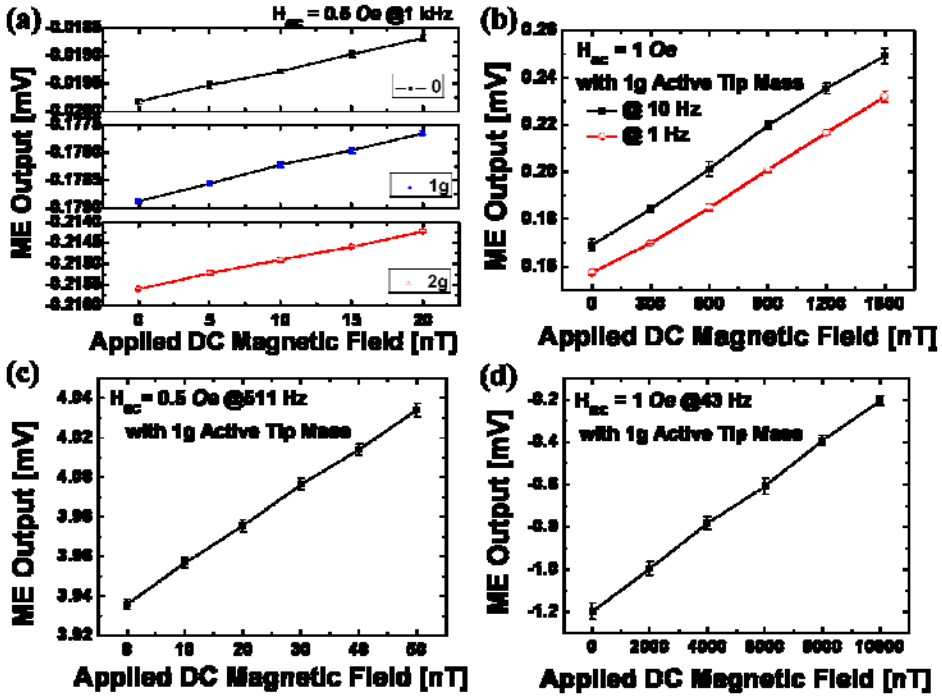

Figure. VIII.4. ME output voltage corresponding to an applied small DC magnetic field: (a) 5 nT under the constant condition of H_{ac}=0.5 Oe at f= 1 kHz with/without active tip mass, (b) 300 nT under H_{ac}= 1 Oe at f= 10 and 1 Hz with 1g active tip mass, (c) and (d) ME response with a 1g active tip mass operating in the 2nd and 1st modes, (c) 10 nT under H_{ac} =0.5 Oe at f= 511 Hz, (d) 2 μT under H_{ac} =0.5 Oe at f= 43 Hz.

Finally, a series of tests were conducted in which small magnetic fields were applied to evaluate the detection limit of the structure. The maximum resolution for detecting a small DC magnetic field was found to be 5 nT under H_{ac} = 0.5 Oe at f= 1 kHz, regardless of active tip mass as shown in Fig. VIII.4(a). The composite can detect

changes in the DC magnetic field as low as 5 nT. The constant resolutions regardless of active tip mass configurations were mainly due to the same slope of the ME responses from 0 to 4.5 Oe, as confirmed in Fig. VIII.2(b). The steep slope from zero to saturation bias provides high sensitivity to a small DC magnetic field. These results confirm the effectiveness of active tip mass. At both 1 and 10 Hz, 300 nT resolution was obtained with 1g tip mass as shown in Fig. VIII.4(b). When we applied small DC bias to the composite at the second resonance of 511 Hz with 1g active tip mass, 10 nT resolution was obtained under H_{ac} = 0.5 Oe at *f*= 1 kHz, as shown in Fig. VIII.4(c). The laminate showed 2 μT resolution at the first bending mode of 43 Hz, as shown in Fig. VIII.4(d). Interestingly, the ME sensing margin at the 2nd resonance is much higher though the detecting resolution is similar to that at 1 kHz. These results clearly show the promise of operating at the second bending mode. The bending resonance can be further lowered by using the combination of dimensionally gradient structures and tip mass. Recent investigations have shown that a flat ME response over a wide frequency range and a magnetic DC bias can be obtained by merging the dimension related bending modes. The magnitude of the ME coefficient can be further enhanced by constructing the MPCPM laminate with in-phase non-hysteretic response, and the sensitivity can be improved by shifting the initial slope of magnetostriction vs. DC bias curve towards low bias values.

IX. Study of Elastic Coupling through Polarization-Magnetic (P-H) Response

In our recent research, we tried to study the ME coupling through a new measurement method in collaboration with **Radiant Technologies Inc.** We demonstrated an automated measurement method for the determination of induced polarization (P) in magnetoelectric composites as a function of applied magnetic field (H) and frequency. The method provides the capability to quantify the changes occurring in the polarization waveform as a function of the pulse width and pulse amplitude with a nanosecond resolution. Using this method, P-H loops were measured over a varying range of frequency and DC magnetic bias, and the data were analyzed in terms of the dissipation occurring during ferroelastic switching. A systematic correlation between the P–H loops and the conventionally measured ME coefficient (dE/dH) was established.

Magnetoelectric (ME) effect defined as the change in dielectric polarization (*P*) under applied magnetic field (*H*) or vice-versa, has been of significant interest in this decade. The induced P is related to the applied H by expression:

$$P = \alpha H \qquad \text{(IX.1)}$$

where α is the second rank ME-suceptibility tensor. Generally, the ME response of composite materials is described by the ME voltage coefficient (α_{ME}) as:

$$\alpha_{ME} = \frac{dE}{dH} \qquad \text{(IX.2)}$$

where $\alpha = \varepsilon_0 \varepsilon_r \alpha_{ME}$ and ε_r is the relative permittivity. It is well-known now that the ME coupling in two-phase composites is achieved through elastic coupling through the interface between the magnetostrictive and piezoelectric materials. In the specific case of piezoelectric – magnetostrictive composites, an optimum magnitude of magnetic DC bias is required in order to achieve a peak ME coefficient under a constant applied AC magnetic field. There are two methods commonly used to evaluate the magnitude of the

ME coefficient: (i) charge amplifier and (ii) lock-in amplifier. Both of these methods provide indirect measurement of α. There is no systematic report in literature on direct measurement of change in the polarization of ME composite under applied DC magnetic field for a macroscopic sample. This imposes serious limitation on our understanding of reversible ME effect in two-phase composites at the bulk scale. We address this issue in this letter and demonstrate a measurement method that can be used in both laboratory and industrial setting to quantitatively determine the magnitude of α_{ME}. Ferroelectric test systems based on the modified Sawyer – Tower technique are commonly used to measure the electric field induced ferroelectric polarization. Thus, improving the sensitivity of ferroelectric testers and reducing the noise factors related to external variables can enable direct measurement of induced polarization through applied magnetic field.

A magnetoelectric laminate composite was synthesized by using the bonding technique. The plate of composition $Pb(Zn_{1/3}Nb_{2/3})_{0.2}(Zr_{0.5}Ti_{0.5})_{0.8}O_3$ [PZNT] with dimensions of 16.5mm × 16.5mm × 1mm were used as the piezoelectric phase. The piezoelectric constant of poled PZNT plates was found to be 500pC/N with dielectric constant of 2219 at 1 kHz. The piezoelectric voltage constant (g_{33}) was measured to be of the order of 23.41×10^{-3} Vm/N. On this PZNT plate, Metglas sheets of 20mm×20mm×100μm dimensions were attached on both sides using epoxy with a curing temperature of 80°C. For the polarization-magnetic field (P-H) loop measurement in longitudinal–transversal (L–T) mode configuration, the Helmholtz coil was used to apply an AC magnetic field (H_{AC}), and an electromagnet was used to apply the DC magnetic field (H_{DC}).

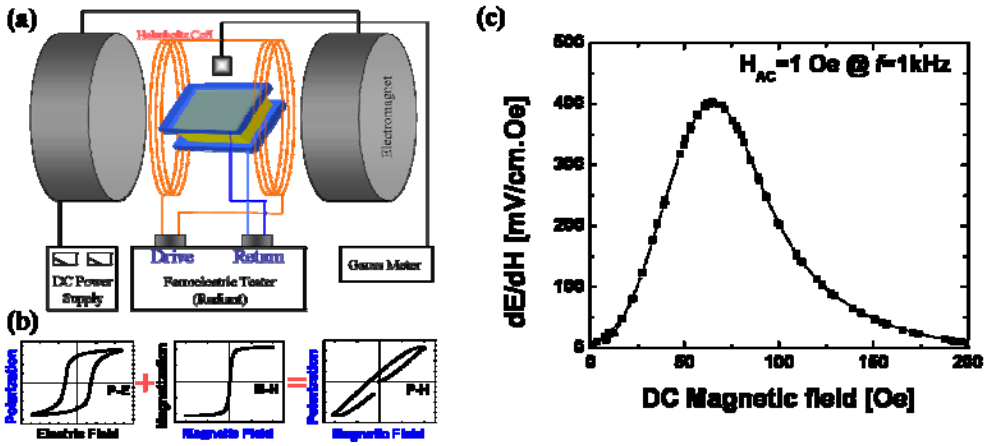

Figure IX.1. (a) Schematic diagram of polarization (P) - magnetic field (H) curve measurement system, (b) Basic concept for P-H measurement, and (c) ME coefficient measured by lock-in amplifier technique.

The induced P under an applied magnetic field was monitored by using a ferroelectric tester (Radiant: Precision Premier II, USA) with configuration shown in Fig. IX.1(a). Figure IX.1 (b) shows the basic concept for the measurement of polarization-magnetic field (P-H) loops using the configuration shown in Fig. IX.1(a). A combinatory measurement of P-E and M-H loops allows direct measurement of the P behavior corresponding to applied H. The sample was placed in the center of a Helmholtz coil which excited H_{AC} from the DRIVE output of the tester, as shown in Fig. IX.1 (a). The output from the sample was connected to the RETURN input of the ferroelectric tester. In

the schematic shown in Fig. IX.1(a), the DC and AC magnetic fields were applied simultaneously to the ME composite. Subsequently, the magnetostrictive material generates strain which is transferred to the piezoelectric capacitor resulting in induced polarization (P). For comparison, the conventional ME measurement was conducted by using a lock-in amplifier technique. Figure IX.1(c) shows the ME response of the synthesized ME composite measured by the lock-in amplifier technique. The peak ME coefficient of 402 mV/cm.Oe was obtained under H_{AC}=1 Oe at *f*=1 kHz and H_{DC}= 63 Oe.

Next, we measured the P-H loops under the condition of H_{AC}=1 Oe at *f*=1 kHz and H_{DC}=63 Oe. Figure IX.2 (a) shows the triangular waveform for applied H_{AC} to the composite and the resulting P response. Two important characteristics can be immediately noticed in this figure: (i) there is a time delay of 52 μ s between the maxima of driving magnetic field and induced polarization indicating the presence of hysteresis, and (ii) the shape of the waveform for induced P was not retraced to that of applied H indicating the curved-shape of hysteresis. Both these factors could be attributed to the losses associated with the transfer of elastic strain (ferroelastic switching), and scattering at the interface due to the presence of surface irregularities and defects. In the case of a laminate composite, the contribution from the later factor is significant.

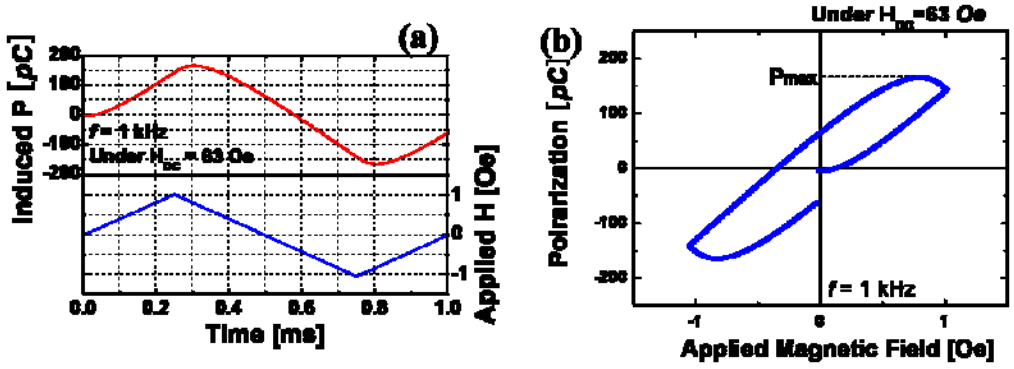

Figure IX.2. (a) Induced polarization and applied magnetic field spectrums as a function of time under H_{AC}= 1 Oe at *f*=1kHz and H_{DC}= 63 Oe, (b) P-H curve under H_{AC}= 1 Oe at *f*=1kHz and H_{DC}= 63 Oe.

Magnetostriction-induced stress oscillation changes the piezoelectric domain states from 180° to 90°, or vice-versa. It favors a ferroelectric tetragonal state with c-axis oriented at 90° from the direction of applied stress. The domains oriented perpendicular to the applied stress grows while those aligned along the direction of stress shrink.[11] Under applied magnetic DC bias the induced magnetostrictive strain (*S*) can be simply given as:

$$S = S_o \exp(i\omega t - i\phi) \qquad \text{(IX.3)}$$

where $S_o = qH_o$, q is the piezomagnetic coefficient, H_o is the amplitude of applied AC magnetic field, ϕ is the phase lag between applied magnetic field and resulting strain, and ω is the angular frequency. The induced polarization (ΔP) at the domain boundaries can be given as:

$$\Delta P = \Delta d\sigma \qquad \text{(IX.4)}$$

where *d* is the piezoelectric coefficient and σ is the applied stress that can be described from Eq. (IX.3) as:

$$\sigma = \sigma_o \exp(i\omega t - i\varphi) \qquad \text{(IX.5)}$$

where $\varphi = \phi + \theta$, and tan θ represents the damping capacity of the material given by the ratio of the stored energy during the deformation to the lost energy as heat. The change in polarization is accompanied by the charge generation at the domain walls which locally induces electric field. Equilibrium is achieved when the generated charge is compensated by the diffusion of mobile charged point defects under the influence of an electric field. This is time–dependent phenomenon which explains the delay in the polarization signal while the local electric field induced deformation is anelastic which explains the shape change. Calculations by Postnikov et al. have shown that for low defect concentration, the relaxation time is given as: $\tau = L^2/\pi^2 D$, where L is the distance between the neighboring domain boundaries and D is the point defect diffusion coefficient. This time constant combined with the interfacial elastic dissipation explains the time-lag observed in measurement.

Figure IX.2 (b) shows the plot of induced polarization as a function of magnetic field amplitude at *f*=1 kHz under H_{DC}= 63 Oe. The hysteresis in this figure clearly shows the nonlinear nature of P which is mostly assumed to be a constant even though Eq. (IX.1) shows the linear relationship between P, α, and H. The maximum polarization (P_{max}) was determined at the point of the flattening of the curve marked in Fig. IX.2 (b), and was of the order of ~160 pC. These results are very interesting, clearly demonstrating the changes in induced polarization of two – phase composites due to magneto-elastic coupling.

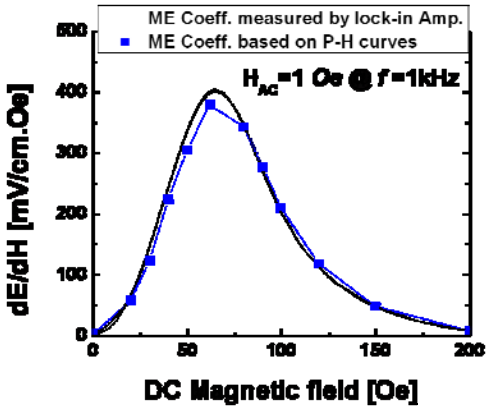

Figure. IX.3. Comparison of ME coefficients evaluated from P-H curves and measured by lock-in amplifier.

The maximum polarization (P_{max}) can be plotted as a function of H_{DC} at a given H_{AC} and frequency. Therefore, the ME coefficient (α_{ME}) can be given as:

$$\therefore \alpha_{ME} = \frac{dE}{dH} = \frac{V_{ME}}{t} = \frac{dP_{\max}}{dH_{AC}} \frac{1}{Ct} \qquad \text{(IX.6)}$$

where t is the thickness of piezoelectric materials. Figure IX.3 compares the computed ME coefficient based on the P-H loops with that determined from the lock-in amplifier technique. The maximum ME coefficient found to be 380 mV/cm.Oe at H_{DC} = 63 Oe, which is in excellent agreement with Fig. IX.1(c). However, this measurement method of induced polarization using the ferroelectric tester provides more precise information and phenomena about the nonlinearity and elastic coupling occurring in the ME composite.

Summary of the achievement

The diagram below summarizes our progress in enhancing the sensitivity of the ME composites through studying for various connectivities from thin film to bulk scale. We have demonstrated several new-types of ME structures to enhance the sensitivity. Finally, our research was able to provide 5nT sensitivity ME composite using conventional sintering process. We have also demonstrated a new mutiferroic measurement method in collaboration with a company which will expedite the development in this field overcoming the limitations of ME measurement.